A leading order imaging series for prestack data acquired over a laterally invariant acoustic medium. Part I: Derivation and preliminary analysis

Simon A. Shaw and Arthur B. Weglein
University of Houston

Abstract

As a multidimensional direct inversion procedure, the inverse scattering series has the ability to image reflectors at their correct spatial location using only the reflection data and an approximate velocity model as input. Therefore, it is a good candidate procedure for deriving an algorithm that can accurately depth image seismic data in complex geological areas where the velocity model is difficult to estimate.

Previously, a subseries of the inverse series was isolated that images reflectors in space without requiring the actual propagation velocity of the medium. This leading order imaging series was found to converge for large contrasts between the actual and reference medium for a 1-D medium and a normal incident plane wave experiment. In this paper (Part I), in preparation for an analysis for data missing low temporal frequency (Part II), the algorithm is formulated for an experiment in which a point source explodes in a three-dimensional constant density acoustic medium where the velocity varies only in depth. The formulation, termed "prestack" in reference to the degree of freedom that exists due to the source-receiver offset, is parameterized for constant angles of incidence.

The leading order imaging series is an approximation to the full depth imaging potential of the inverse series in that it is leading order in the data. The first term in the series images reflectors at the depths dictated by the constant reference velocity and the data's travel times. The remaining terms use the data's amplitudes and travel times as well as the reference velocity to shift the reflectors closer to their correct location in depth.

Analytic and numerical examples are used to demonstrate that, for small contrasts between the actual and reference medium, the leading order imaging series significantly improves the predicted depths of the reflectors at precritical angles, effectively flattening the angle gathers. For higher contrasts, or when greater accuracy is desired, then higher order imaging terms are required that go beyond the leading order terms identified and analyzed in this paper.

1 Introduction (motivation and background)

Depth imaging of seismic reflection data plays a critical role in the exploration and production of oil and gas. The primary goal of depth imaging is to produce a spatially accurate map of reflectors below the earth's surface. This structural map is important to the oil and gas industry because it plays a key role in determining where to drill for hydrocarbon reserves, which has an enormous economic, environmental and political impact.

Current depth imaging algorithms can be formulated from a linear inverse scattering model, in which the reference velocity is assumed to be close enough to the actual velocity in order to place reflectors at their correct spatial locations. In practice, especially in complex geological environments, the most accurate methods for deriving the reference velocity model may be inadequate for linear imaging algorithms inasmuch as they fail to focus the reflection energy at the correct location. The inverse scattering series has the ability to image primary reflection events at their correct location using only the reflection data and an approximate reference velocity model (Weglein et al., 2000). The first term in the inverse series is a linear inversion of the data. It uses a velocity model that is incorrect below the measurement surface to image reflectors at locations expected when imaging with a typical depth imaging algorithm (essentially with the equation depth = velocity $\times$ travel time). Therefore, in general, the first term in the series will mislocate the reflectors unless the velocity model is correct. The higher order terms in the inverse series, that are non-linear in the data, contain parts that move the reflectors to their true spatial locations. These non-linear imaging terms only exist when the velocity model is incorrect. In fact, the inverse series only exists when the reference and actual media are different.

As a multidimensional direct inversion procedure, the inverse scattering series has more to do than image reflectors at their correct locations in space. The inverse series removes multiply reflected events, images reflectors, and inverts amplitudes for medium parameters *directly* using only the measured data and a reference medium's parameters (Moses, 1956; Razavy, 1975; Stolt and Jacobs, 1980; Weglein et al., 1981). Early numerical tests of the inverse series' ability to directly invert seismic data (Jacobs, 1980; Carvalho, 1992) suggested that it converged only when the reference medium properties were very close to the actual medium properties. Multiples were a significant impediment to estimating the earth's properties (and deriving an adequate reference medium) from seismic reflection data. As a result, research was undertaken into using the inverse series to derive algorithms that removed free-surface and internal multiples from seismic data, but that stopped short of imaging and parameter estimation. The strategy employed was to isolate subseries of the inverse series that are responsible for removing multiples.

Weglein et al. (1997) have derived multidimensional free surface and internal multiple attenuation algorithms by isolating separate subseries of the inverse series that perform these two tasks. These subseries turned out to have more favorable convergence properties than the entire inverse series. The algorithms converge for an acoustic reference medium of water and they share the advantage of not requiring information about the earth below the measurement surface. An important prerequisite of all inverse series algorithms is that the source wavelet is known. These multiple attenuation algorithms are now routinely used in seismic processing to remove multiples prior to velocity estimation, imaging and AVO analysis. A key concept within the subseries approach to inversion of seismic data, is to apply the task-specific algorithms in the following order: 1.) free surface multiple removal; 2.) internal multiple removal; 3.) depth imaging and 4.) target identification. In taking this staged approach, each step is less ambitious than direct inversion for earth properties and is therefore likely to be less demanding of the input data, reference medium proximity, and of computational requirements. In addition, the subseries are allowed to benefit from all of the tasks that have been achieved earlier in the sequence, thus further simplifying the problem at each step. For a comprehensive review of the inverse scattering series and its application to seismic exploration, see Weglein et al. (2003).

The strategy employed in developing inverse scattering subseries algorithms to solve problems in seismic data processing has been to first consider the simplest situation in which the particular problem exists. Most often this is a 1-D normal incidence experiment in a constant-density acoustic medium. The simplest reference medium is chosen that agrees with the actual medium above the measurement surface and confines the perturbation to be below the receivers. Then the inverse series is analytically computed and a subseries is sought that is responsible for achieving the specific processing task (one of the four listed above). The subseries is isolated through a combination of intuition and experience garnered through studying the forward series terms that construct the seismic wavefield.

If the subseries algorithm demonstrates an intrinsic ability to achieve its objective, then it is reformulated and generalized so that it may eventually be tested on multidimensional field data. Shaw et al. (2003) considered the simple situation of a normal-incidence experiment over a 1-D constant density acoustic medium for which the velocity was an unknown function of depth. An imaging series algorithm was derived that imaged reflectors in depth using a constant reference velocity and it was shown analytically that this series converged for large finite contrasts between the actual and reference velocities. For relatively small contrasts, the leading order imaging series is a good approximation to the entire imaging series in that the predicted depths are a significant improvement over linear depth imaging with the reference velocity. It was also demonstrated that this series converges more quickly for smaller contrasts and for lower maximum frequencies. Therefore, a proximate reference velocity and a source spectrum with a lower maximum frequency both aid the rate of convergence.

Having established for the simplest examples that the leading order imaging series has good convergence properties, the next stage in developing a practical algorithm is to evaluate its performance under increasingly realistic conditions. Since seismic data are always frequency bandlimited, one of the highest priority tests involves an analysis of the algorithm under conditions of missing low frequencies. Such an analysis is provided by Shaw and Weglein (2004) in a second paper (Part II). In preparation for that analysis, the leading order imaging series algorithm is rederived here to accommodate prestack input data. The offset aperture in prestack data provides a lower vertical wavenumber k_z and more closely resembles the actual seismic experiment. This paper includes a derivation of the prestack leading order imaging series and presents some preliminary analytic and numerical examples. These examples are used to discuss how the imaging series performs the task of depth imaging given a constant reference velocity that is never updated.

We consider a 3-D constant density acoustic medium with point sources and receivers located at $\vec{x}_s = (x_s, y_s, z_s)$ and $\vec{x}_g = (x_g, y_g, z_g)$, respectively. Wave propagation in this medium can be characterized by the wave equation

$$\left(\nabla^2 + \frac{\omega^2}{c^2(\vec{x}_g)}\right) P(\vec{x}_g|\vec{x}_s;\omega) = -A(\omega)\delta(\vec{x}_g - \vec{x}_s) \tag{1}$$

where P is the pressure field, A is the source wavelet, c is the propagation velocity and ω is the angular frequency. The temporal Fourier transform is defined by

$$P(\vec{x}_g|\vec{x}_s;\omega) = \int_{-\infty}^{\infty} P(\vec{x}_g|\vec{x}_s;t)e^{i\omega t}dt. \tag{2}$$

To simplify the current analysis of the prestack imaging series, we will be assuming that the medium varies only in the z direction. For the generalization to a 2-D earth, see Liu et al. (2004). The velocity, c, can be expressed in terms of a constant reference velocity, c_0, and a perturbation, α, such that

$$\frac{1}{c^2(z)} = \frac{1}{c_0^2}\left(1 - \alpha(z)\right). \tag{3}$$

For this acoustic problem, the goal of inversion is to solve for α which can be written as an infinite series

$$\alpha = \alpha_1 + \alpha_2 + \alpha_3 + \cdots \tag{4}$$

where α_1, the first term in the series for α, is linearly related to the scattered field, $P_s = P - P_0$. P_0 is the pressure wavefield due to the same source, $A(\omega)$, in the reference medium, i.e., a wholespace with velocity, c_0. The second term, α_2, is quadratic in P_s, the third term, α_3, is cubic and so on. After using the inverse series (4) to solve for α, we can use (3) to solve for the unknown velocity, $c(\vec{x})$. The objective of the research described here is in fact not to solve for the medium parameters (in this case just c), but to solve directly for the *location* at which the perturbation α changes. This is the problem of imaging in a medium whose velocity is not known before or after the imaging procedure.

2 A leading order imaging series for a 3-D experiment over a laterally invariant acoustic medium

2.1 The first term, α_1, and its degree of freedom

If the source wavelet is deconvolved so that $\tilde{D} = P_s/A$, then $\tilde{D}$ is related to α_1 by

$$\tilde{D}(\vec{x}_g|\vec{x}_s;\omega) = \int_{-\infty}^{\infty} G_0(\vec{x}_g|\vec{x}\,';\omega)\, k_0^2\alpha_1(\vec{x}\,')\, G_0(\vec{x}\,'|\vec{x}_s;\omega)\, d\vec{x}\,' \tag{5}$$

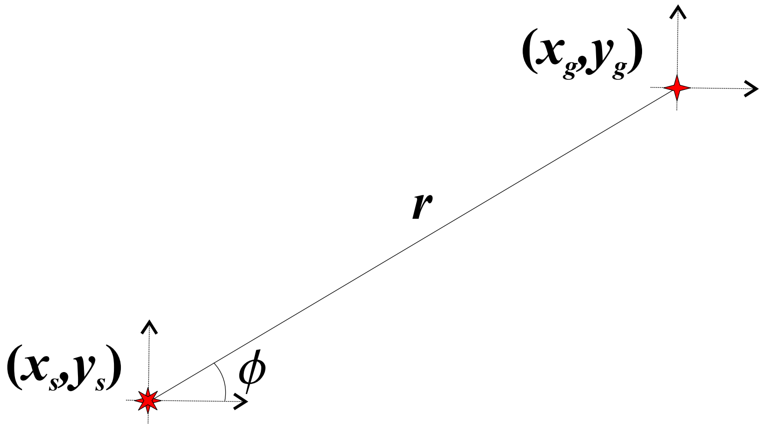

Figure 1: *Plan view showing the relationship between the horizontal cartesian and cylindrical coordinates. r is the source-receiver offset in the horizontal plane and ϕ is the azimuth. For a 1-D subsurface, the data are invariant in azimuth.*

where $k_0 = \omega/c_0$ and G_0 is the causal Green's function satisfying the wave equation in the reference medium. The solution for α_1 in cylindrical coordinates is (see Appendix A)

$$\tilde{\alpha}_1(-2q_g) = 2\pi \frac{-4q_g^2}{k_0^2} e^{iq_g(z_g+z_s)} \int_0^\infty \tilde{D}(r;\omega) J_0(k_r r) r dr \tag{6}$$

where the vertical and horizontal wavenumbers, q_g and k_r, respectively, are related by

$$q_g = \frac{\omega}{c_0}\sqrt{1 - \frac{k_r^2 c_0^2}{\omega^2}}. \tag{7}$$

$J_0(k_r r)$ is a zero order Bessel function of the first kind that arises due to the azimuthal symmetry and is

$$J_0(k_r r) = \frac{1}{2\pi}\int_0^{2\pi} e^{ik_r r cos\phi'} d\phi'. \tag{8}$$

Figure 1 illustrates the relationship between the horizontal cartesian coordinates (x_g, y_g) and cylindrical coordinates (r, ϕ).

The fact that the data are a function of both time and source-receiver offset whereas α is only a function of depth is evident in (6) in that $\tilde{\alpha}_1$ is over-determined. Whereas $\tilde{\alpha}_1$ is only a function of q_g, the right-hand side of (6) can be written as a function of two independent variables, e.g., (q_g, ω) or (k_r, ω). Large angles of incidence can construct $\tilde{\alpha}_1$ at low q_g values since $q_g = k_0 \cos\theta_0$. Inverse Fourier transforming both sides of (6) gives

$$\begin{aligned}\alpha_1(z) =& \frac{2}{2\pi}\int_{-\infty}^{\infty} \tilde{\alpha}_1(-2q_g) e^{-2iq_g z} dq_g \\ =& -8 \int_{-\infty}^{\infty} \frac{q_g^2}{k_0^2} e^{-iq_g(2z-(z_g+z_s))} \int_0^\infty \tilde{D}(r;\omega) J_0(k_r r) r dr dq_g\end{aligned} \tag{9}$$

where $q_g^2/k_0^2 = \cos^2\theta_0$. Considering fixed angles of incidence, θ_0, leads to a number of different estimates of α_1, denoted by $\alpha_1(z,\theta_0)$. Fixing θ_0 is the same as fixing horizontal and vertical slownesses, p_0 and ζ_0, respectively, where

$$p_0 = \frac{\sin\theta_0}{c_0} \text{ and } \zeta_0 = \frac{\cos\theta_0}{c_0}.$$

However, q_g is still allowed to vary through the variation in ω since $q_g = \omega\zeta_0$. We proceed by changing variables from q_g to ω:

$$\alpha_1(z,\theta_0) = -\,8\zeta_0\cos^2\theta_0 \int_{-\infty}^{\infty} e^{-i\omega\zeta_0(2z-(z_g+z_s))} \int_0^{\infty} \tilde{D}(r;\omega) J_0(\omega p_0 r) r dr d\omega. \tag{10}$$

Defining $\tau_0 = \zeta_0\,(2z-(z_g+z_s))$ and performing the inverse temporal Fourier transform of the data $\tilde{D}(r;\omega)$, (10) becomes

$$\alpha_1(z,\theta_0) = -\,8\zeta_0\cos^2\theta_0 \int_0^{2\pi}\int_0^{\infty} D(r;\tau_0 - p_0 r\cos\phi) r dr d\phi. \tag{11}$$

Changing back to cartesian coordinates yields (see Appendix A)

$$\alpha_1(z,\theta_0) = -\,8\zeta_0\cos^2\theta_0 \int_{-\infty}^{\infty}\int_{-\infty}^{\infty} D(x_g,y_g;\tau_0 - x p_0) dx_g dy_g. \tag{12}$$

Equation (12) is recognizable as a scaled slant stack of the recorded data (Treitel et al., 1982). In cartesian coordinates, it requires sums in both the x and y directions, whereas in cylindrical coordinates, as a result of the symmetry of a laterally invariant medium, these integrals are replaceable by integrals over ϕ and r (11) or ω and r (10). An alternative approach to handling the degree of freedom in (9) is to hold ω fixed and integrate over angle or vertical slowness $\zeta_0 = \cos\theta/c_0 = q_g/\omega$. This parameterization will result in different estimates of α_1 for constant ω values and is the subject of ongoing research.

2.2 Task separation in the second and third terms

The integral equation for the second term in the inverse series for this acoustic problem is

$$\begin{aligned}\int_{-\infty}^{\infty} G_0\left(\vec{x}_g|\vec{x}\,';\omega\right) k_0^2\alpha_2(\vec{x}\,') G_0\left(\vec{x}\,'|\vec{x}_s;\omega\right) d\vec{x}\,' \\ = -\int_{-\infty}^{\infty} d\vec{x}\,' \, G_0\left(\vec{x}_g|\vec{x}\,';\omega\right) k_0^2\alpha_1(\vec{x}\,') \\ \times \int_{-\infty}^{\infty} d\vec{x}\,''\, G_0\left(\vec{x}\,'|\vec{x}\,'';\omega\right) k_0^2\alpha_1(\vec{x}\,'') G_0\left(\vec{x}\,''|\vec{x}_s;\omega\right).\end{aligned} \tag{13}$$

The solution to (13) is detailed in Appendix B where $\tilde{\alpha}_2$ as a function of vertical wavenumber is shown to be

$$\tilde{\alpha}_2(-2q_g) = -\int_{-\infty}^{\infty} dz' e^{2iq_g z'} \frac{k_0^2}{2q_g^2} \left(\alpha_1^2(z') + \int_0^{z'} dz'' \alpha_1(z'') \frac{d\alpha_1(z')}{dz'} \right). \tag{14}$$

As in the case of $\tilde{\alpha}_1$, there is a degree of freedom in (14) that results in a choice of which variable to hold constant, and which to integrate over in the construction of $\alpha_2(z)$. For example, if we choose to keep incident angle θ_0 constant, then performing the inverse Fourier transform of (14) gives

$$\alpha_2(z,\theta_0) = -\frac{1}{2\cos^2\theta_0} \left(\alpha_1^2(z,\theta_0) + \int_0^{z} dz' \alpha_1(z',\theta_0) \frac{\partial \alpha_1(z,\theta_0)}{\partial z} \right) \tag{15}$$

since

$$\frac{k_0^2}{q_g^2} = \frac{k_0^2}{k_0^2\cos^2\theta} = \frac{1}{\cos^2\theta}.$$

The second term in the inverse series (15) has been separated into the sum of two pieces. As explained by Weglein et al. (2002), these two terms have distinctly different roles in the inversion procedure. The first piece

$$\alpha_{21}(z,\theta_0) = -\frac{1}{2\cos^2\theta_0} \alpha_1^2(z,\theta_0) \tag{16}$$

is responsible for correcting the amplitude of $\alpha_1(z,\theta_0)$ (see, e.g., Zhang and Weglein, 2004) and the second piece

$$\alpha_{22}(z,\theta_0) = -\frac{1}{2\cos^2\theta_0} \int_{-\infty}^{z} \alpha_1(z',\theta_0) dz' \frac{\partial \alpha_1(z,\theta_0)}{\partial z} \tag{17}$$

acts to shift the mislocated interfaces in $\alpha_1(z,\theta_0)$ closer to their true depths. This shift is accomplished by a Taylor series for the difference of two Heaviside functions expanded about the depth of each mislocated interface. The first term in this Taylor series for the shift is α_{22}. For details on this expansion, the reader is referred to Weglein et al. (2002).

Proceeding to the third term in the series, the integral equation to be solved is

$$\begin{aligned}
&\int_{-\infty}^{\infty} d\vec{x}'\, G_0\left(\vec{x}_g|\vec{x}';\omega\right) k_0^2 \alpha_3(z') G_0\left(\vec{x}'|\vec{x}_s;\omega\right) \\
&\quad = -\int_{-\infty}^{\infty} d\vec{x}'\, G_0\left(\vec{x}_g|\vec{x}';\omega\right) k_0^2 \alpha_1(z') \int_{-\infty}^{\infty} d\vec{x}''\, G_0\left(\vec{x}'|\vec{x}'';\omega\right) k_0^2 \alpha_2(z'') G_0\left(\vec{x}''|\vec{x}_s;\omega\right) \\
&\quad\quad -\int_{-\infty}^{\infty} d\vec{x}'\, G_0\left(\vec{x}_g|\vec{x}';\omega\right) k_0^2 \alpha_2(z') \int_{-\infty}^{\infty} d\vec{x}''\, G_0\left(\vec{x}'|\vec{x}'';\omega\right) k_0^2 \alpha_1(z'') G_0\left(\vec{x}''|\vec{x}_s;\omega\right) \\
&\quad\quad -\int_{-\infty}^{\infty} d\vec{x}'\, G_0\left(\vec{x}_g|\vec{x}';\omega\right) k_0^2 \alpha_1(z') \int_{-\infty}^{\infty} d\vec{x}''\, G_0\left(\vec{x}'|\vec{x}'';\omega\right) k_0^2 \alpha_1(z'') \\
&\quad\quad \times \int_{-\infty}^{\infty} d\vec{x}'''\, G_0\left(\vec{x}''|\vec{x}''';\omega\right) k_0^2 \alpha_1(z''') G_0\left(\vec{x}'''|\vec{x}_s;\omega\right).
\end{aligned} \tag{18}$$

The solution for $\alpha_3(z)$ can be broken into a number of pieces two of which are given in Appendix C. This separation is discussed in Shaw et al. (2003) for the normal incidence case and it is extendable to prestack data when the angle θ_0 is held constant. The amplitude correction and leading order imaging contributions from the third term are given by:

$$\alpha_3(z,\theta_0) = \frac{1}{\cos^4\theta_0}\left[\frac{3}{16}\alpha_1^3(z,\theta_0) + \frac{1}{8}\left(\int_0^z \alpha_1(z',\theta_0)dz'\right)^2 \frac{\partial^2\alpha_1(z,\theta_0)}{\partial z^2} + \cdots\right]. \tag{19}$$

2.3 A prestack leading order imaging series

The imaging series is a subseries of the inverse series that is responsible for positioning reflectors at their correct spatial location (Weglein et al., 2000, 2002). For the problem considered here, in which the earth is characterized by a single parameter, the imaging series is written

$$\alpha^{\mathrm{IM}} = \alpha_1^{\mathrm{IM}} + \alpha_2^{\mathrm{IM}} + \alpha_3^{\mathrm{IM}} + \cdots \tag{20}$$

where α_i^{IM} is the term in the imaging series that is i^{th} order in the scattered field and is found in the i^{th} term of the inverse series. The leading order imaging series, α^{LOIM}, is the contribution to the imaging series that is leading order in the scattered field. The terms in this imaging series have been found to exhibit a specific pattern (corresponding to particular scattering diagrams) recognized by Shaw et al. (2003) which allowed the prediction of a general form. Following that earlier work, and using the constant-θ_0 formulation, the prestack form of the algorithm is

$$\begin{aligned}\alpha^{\mathrm{LOIM}}(z,\theta_0) =& \alpha_1(z,\theta_0) - \frac{1}{2}\frac{1}{\cos^2\theta_0}\left(\int_0^z \alpha_1(z',\theta_0)dz'\right)\frac{\partial\alpha_1(z,\theta_0)}{\partial z} \\ &+ \frac{1}{8}\frac{1}{\cos^4\theta_0}\left(\int_0^z \alpha_1(z,\theta_0)dz'\right)^2 \frac{\partial^2\alpha_1(z,\theta_0)}{\partial z^2} - \cdots \\ =& \sum_{n=0}^{\infty}\frac{(-1/2)^n}{n!\cos^{2n}\theta_0}\left(\int_0^z \alpha_1(z',\theta_0)dz'\right)^n \frac{\partial^n\alpha_1(z,\theta_0)}{\partial z^n}\end{aligned} \tag{21}$$

where

$$\alpha_1(z,\theta_0) = -8\zeta_0\cos^2\theta_0 \int_0^{2\pi}\int_0^{\infty} D(r;\tau_0 - p_0 r\cos\phi)rdrd\phi.$$

Performing a Fourier transform of (21) gives

$$\begin{aligned}\alpha^{\mathrm{LOIM}}(k_z,\theta_0) =& \int_{-\infty}^{\infty}\sum_{n=0}^{\infty}\frac{(-ik_z/(2\cos^2\theta_0))^n}{n!}\left(\int_0^z \alpha_1(z',\theta_0)dz'\right)^n \alpha_1(z,\theta_0)e^{-ik_z z}dz \\ =& \int_{-\infty}^{\infty}\exp\left[-ik_z/(2\cos^2\theta_0)\int_0^z \alpha_1(z',\theta_0)dz'\right]\alpha_1(z,\theta_0)e^{-ik_z z}dz.\end{aligned} \tag{22}$$

where the power series

$$\sum_{n=0}^{\infty} \frac{\left[-ik_z/(2\cos^2\theta_0)\int_0^z \alpha_1(z',\theta_0)dz'\right]^n}{n!} = \exp\left[-ik_z/(2\cos^2\theta_0)\int_0^z \alpha_1(z',\theta_0)dz'\right] \quad (23)$$

was substituted to arrive at (22). Inverse Fourier transforming both sides of (22) yields a closed form for the leading order imaging series that operates θ_0-by-θ_0 (or p_0-by-p_0):

$$\alpha^{\mathrm{LOIM}}(z,\theta_0) = \alpha_1\left(z - 1/(2\cos^2\theta_0)\int_0^z \alpha_1(z',\theta_0)dz', \theta_0\right). \quad (24)$$

The prestack leading order imaging series for a point source in a laterally invariant acoustic medium can be implemented by slant-stacking (or τ-p transforming) the data, weighting each p trace by the factor $-8\zeta_0\cos^2\theta_0$, and then operating on each trace with the formula provided in (24). When $\theta_0 = 0$, (21) and (24) reduce to the normal incidence algorithms given by Shaw et al. (2003). The normal incidence leading order imaging series was shown to converge for arbitrarily large finite contrasts between the actual and reference medium. From (23), it can be concluded that the rate of convergence of (21) will be greater for smaller values of k_z, smaller values of $\int_0^z \alpha_1(z',\theta_0)dz'$, and smaller values of θ_0. Analysis of the 1-D normal incidence algorithm showed that, for relatively small contrasts (the actual velocity within about 10% of the reference velocity), the leading order contributions to the imaging series can accurately locate reflectors. Higher contrasts or greater accuracy require higher order imaging terms.

3 Analytic and numerical examples

3.1 Analytic example with two interfaces; leading and higher order imaging terms

Consider a model that consists of two horizontal interfaces at depths z_a and z_b and a discontinuous velocity profile c_0-c_1-c_2 (Fig. 2). The wavefield in the upper halfspace, Ψ_0, consists of an incident field, Ψ_i, and a reflected field, Ψ_r. The measured reflected wavefield can be derived by decomposing the incident field into a sum of plane waves (the Sommerfeld integral) and then matching boundary conditions at each interface. The result is

$$\Psi_r(r,z_g;\omega) = i\omega\int_0^{\infty} \frac{\left(R_{01} + T_{01}R_{12}T_{10}e^{2i\omega\zeta_1(z_b-z_a)} + \cdots\right)}{\zeta_0} e^{i\omega\zeta_0(2z_a-z_s-z_g)} J_0(\omega p_0 r)p_0 dp_0 \quad (25)$$

where the reflection and transmission coefficients are functions of angle and are given by

$$R_{01} = \frac{\zeta_0-\zeta_1}{\zeta_0+\zeta_1}, T_{01} = \frac{-2\zeta_1}{\zeta_0+\zeta_1}, R_{12} = \frac{\zeta_1-\zeta_2}{\zeta_1+\zeta_2} \text{ and } T_{10} = \frac{2\zeta_0}{\zeta_0+\zeta_1}. \quad (26)$$

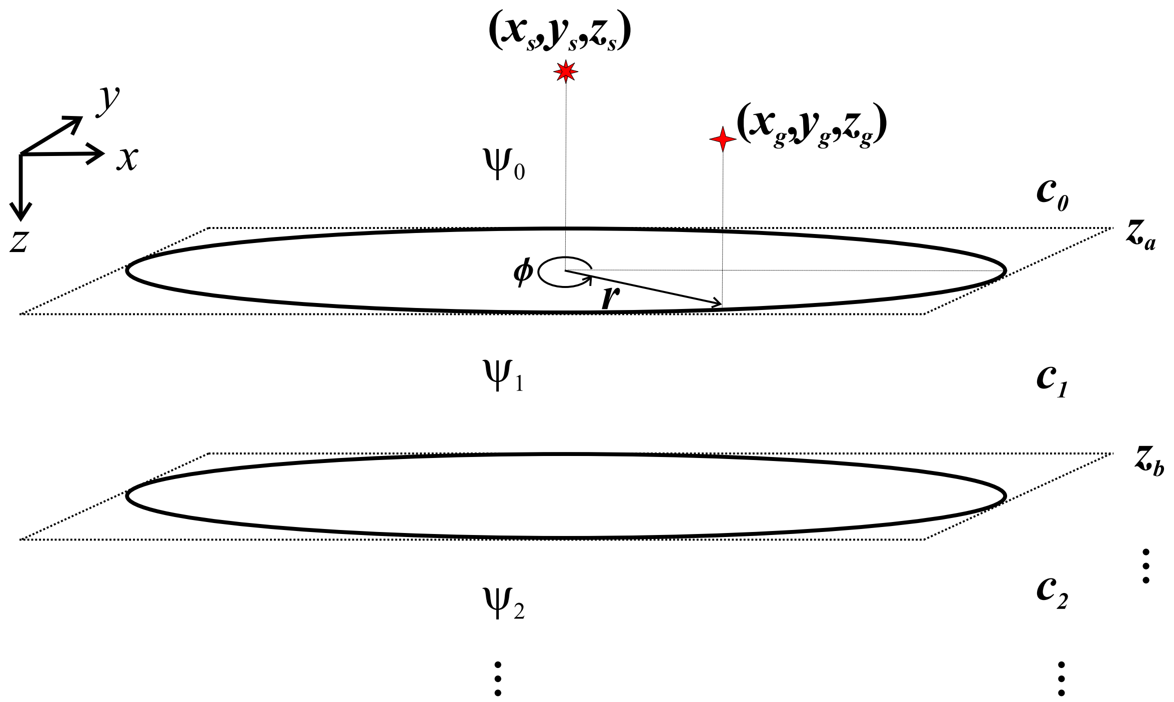

Figure 2*: A multi-layer 1-D constant density acoustic model. In the absence of a free surface, all reflected waves at the receiver are upgoing.*

We further define $R'_{12} = T_{01}R_{12}T_{10}$. The vertical slownesses are functions of the incident angles in each layer since

$$\zeta_i = \frac{\cos\theta_i}{c_i} \ , \ \ i = 0, 1, 2, \ldots \tag{27}$$

The "$+\cdots$" in (25) are the internal multiple reflections in the data. The internal multiple removal subseries, that begins in the third term of the inverse series, is assumed to have been applied before the imaging subseries. This results in a new effective data and a new effective α_1 that contain only primary reflection events. This step is part of the strategy of inverse series task separation described by Weglein et al. (2003). For the two reflector example considered here, the internal multiples are of no consequence since the imaging series only uses information recorded earlier than the primary event being imaged, which excludes the multiples. Reverting to the symbol $\tilde{D}$ for data that contain only primary reflections, and changing the integration variable from p_0 to k_r, (25) becomes

$$\tilde{D}(r;\omega) = -\int_0^\infty \frac{\left(R_{01} + R'_{12}e^{2i\omega\zeta_1(z_b - z_a)}\right)}{i\omega\zeta_0} e^{i\omega\zeta_0(2z_a - z_s - z_g)} J_0(k_r r) k_r dk_r \tag{28}$$

Substituting the data (28) into the linear inverse equation (10), then for this two-reflector example, the first term in the series for $\alpha(z)$ can be written as a function of angle

$$\begin{aligned}\alpha_1(z,\theta_0) =& -8\zeta_0\cos^2\theta_0\int_{-\infty}^{\infty}e^{-i\omega\zeta_0(2z-(z_g+z_s))}\int_0^{\infty}\tilde{D}(r;\omega)J_0(k_r r)rdrd\omega\\ =&8\cos^2\theta_0\int_{-\infty}^{\infty}\frac{R_{01}+R'_{12}e^{2i\omega\zeta_1(z_b-z_a)}}{i\omega\zeta_0}e^{-2i\omega\zeta_0(z-z_a)}d\omega\\ =&4\cos^2\theta_0\left[R_{01}H\left(z-z_a\right)+R'_{12}H\left(z-z_{b'}\right)\right] \end{aligned} \tag{29}$$

where the shallower reflector is correctly located at z_a (since the velocity down to z_a was correct) but the deeper reflector is mislocated at depth

$$z_{b'} = z_a + (z_b - z_a)\frac{\zeta_1}{\zeta_0}. \tag{30}$$

Therefore, the correction in the depth of the second reflector from $z_{b'}$ to the actual depth z_b is

$$\begin{aligned} z_b - z_{b'} &= z_b - z_a - (z_b - z_a)\frac{\zeta_1}{\zeta_0}\\ &= (z_b - z_a)\left(1-\frac{\zeta_1}{\zeta_0}\right). \end{aligned} \tag{31}$$

Substituting (30) into (31) to eliminate z_b on the right-hand side gives

$$z_b - z_{b'} = (z_{b'} - z_a)\left(\frac{\zeta_0}{\zeta_1}-1\right). \tag{32}$$

The ratio of the slownesses can be written as an infinite series in the reflection coefficient (or amplitude) of the shallower reflector under the condition that $|R_{01}| < 1$. This condition precludes post-critical reflections. Therefore,

$$\frac{\zeta_0}{\zeta_1} = \frac{(1-R_{01})}{(1+R_{01})} = 1 - 2R_{01} + 2R_{01}^2 - 2R_{01}^3 + \cdots\ , |R_{01}| < 1.$$

Hence, the shift from the depth predicted by the first term in the series ($z_{b'}$) to the actual depth of the second reflector (z_b) can be expressed, for precritical angles, as

$$z_b - z_{b'} = -2(z_{b'} - z_a)\left(R_{01} - R_{01}^2 + R_{01}^3 - \cdots\right). \tag{33}$$

The approximation to this shift that is leading order in the data's amplitudes is

$$z_b - z_{b'} \approx -2(z_{b'} - z_a)R_{01}. \tag{34}$$

This is equal to the shift calculated automatically by the leading order imaging series. To see this, we substitute the first term in the imaging series for this example (29) into the closed form for α^{LOIM} (24) and evaluate the algorithm at $z_{b'}$

$$\begin{aligned}\alpha^{\text{LOIM}}(z_{b'},\theta_0) =&\alpha_1\left(z_{b'}-1/(2\cos^2\theta_0)\int_0^{z_{b'}}\alpha_1(z',\theta_0)dz',\theta_0\right)\\ =&\alpha_1\left(z_{b'}-2\int_0^{z_{b'}}R_{01}\left(\theta_0\right)H\left(z'-z_a\right)dz'-2\underbrace{\int_0^{z_{b'}}R'_{12}\left(\theta_0\right)H\left(z'-z_{b'}\right)dz'}_{=0}\right)\\ =&\alpha_1\left(z_{b'}-2\left(z_{b'}-z_a\right)R_{01}\left(\theta_0\right)\right).\end{aligned}\tag{35}$$

We see from (35) that the leading order imaging series α^{LOIM} shifts the interface at $z_{b'}$ in α_1 to a new depth $z_{b'}+2\left(z_{b'}-z_a\right)R_{01}$ which is closer to the actual depth z_b. As might be expected, this shift is a function of angle.

The extent to which the leading order imaging series, α^{LOIM}, is a good approximation to the entire imaging series, α^{IM}, depends on the magnitude of the perturbation above the reflector being imaged. Higher order imaging series that go beyond the leading order approximation include successively more amplitude terms in the series for the shift in (33). For models containing more than two interfaces, the leading order order imaging series produces an approximation to the shift at each mislocated interface that is an infinite series in reflection *and transmission* coefficients in the overburden. It is postulated that higher terms in the imaging series will act to unravel these transmission coefficients.

Consider two specific examples where the reference velocity $c_0 = 1500$ m/sec and the two reflectors are located at $z_a = 1000$ m and $z_b = 1075$ m. In the first case $c_1 = 1650$ m/sec and in the second case $c_1 = 1350$ m/sec. Figure 3 illustrates the depths predicted by the first term in the series and three approximations to the imaging series for two different velocity models. The variation of $z_{b'}$ with angle is referred to as residual moveout. At higher angles, the depth of the second reflector predicted by the first term in the series is less accurate. This is because the constituent plane waves travelling at higher angles of incidence spend a proportionally longer time in the layer with the wrong velocity. Therefore, the non-linear terms in the imaging series have to shift the interface further at higher angles. The fact that the magnitude of the reflection coefficient at the first interface, $|R_{01}|$, increases with angle aids the imaging terms in shifting greater distances with angle. On the other hand, this increase in amplitude will tend to make the leading order approximation in (34) less justifiable. Figure 3 shows, for two examples, that including higher order imaging terms improves the accuracy of the predicted depth, especially at higher angles where they are needed more. Figure 4 shows two more examples where the contrasts are twice as large as in Fig. 3. These examples show how higher order imaging terms become more important for higher contrasts between the actual and reference velocity.

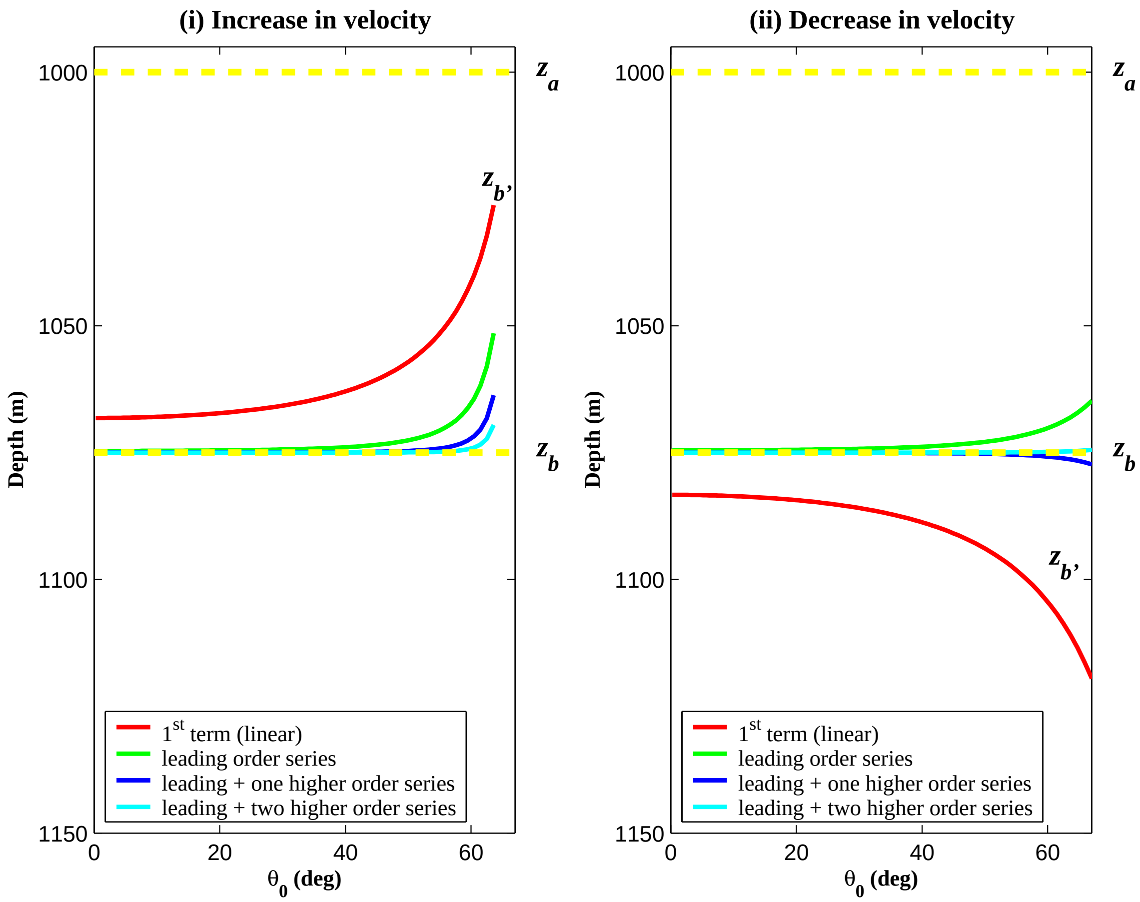

Figure 3: *Low contrast analytic example. Depths predicted by the first term in the series and three different imaging series as a function of angle for two specific analytic examples:* $z_a = 1000$ *m,* $z_b = 1075$ *m,* $c_0 = 1500$ *m/sec and* $c_1 = 1650$ *m/s (i),* $c_1 = 1350$ *m/sec (ii).*

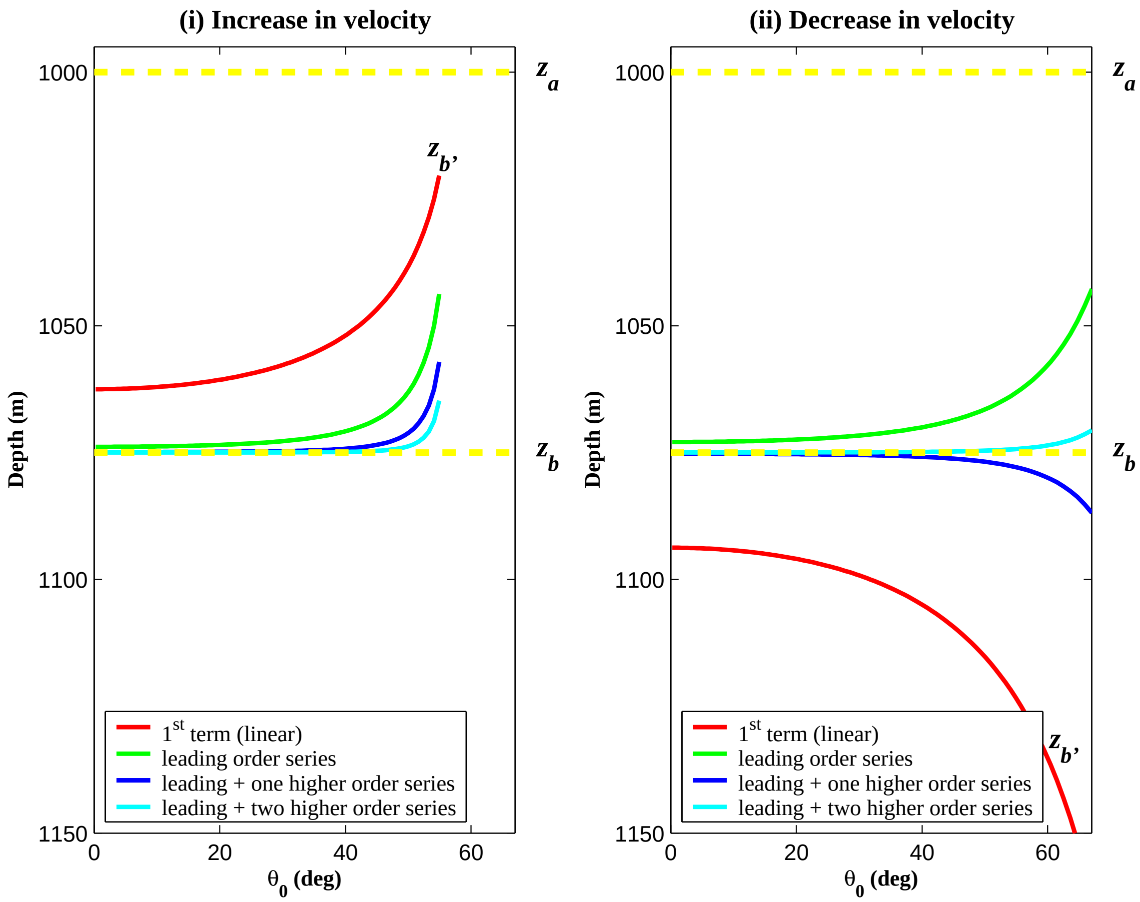

Figure 4: *High contrast analytic example. Depths predicted by the first term in the series and three different imaging series as a function of angle for two specific analytic examples:* $z_a = 1000$ *m,* $z_b = 1075$ *m,* $c_0 = 1500$ *m/sec and* $c_1 = 1800$ *m/sec (i),* $c_1 = 1200$ *m/sec (ii).*

3.2 Numerical examples

We test the leading order imaging series on data synthesized using a reflectivity algorithm (see, for example, Kennett (1983)). The source wavelet is a band-limited delta function with a frequency spectrum $A(f)$ where $f_{min} < f < f_{max}$. We begin with the simplest imaging problem of two reflectors in a constant density acoustic medium with no free surface.

As with the analytic examples, two specific cases are considered, one representing the case where the reference velocity is slower than the actual velocity, and one where the reference velocity is faster. In the former example, the velocities are $c_0 = 1500$ m/s, $c_1 = 1650$ m/s and $c_2 = 1500$ m/s, and so the critical angle for a downgoing plane wave at the first interface is 65°. In the latter example, the velocities are $c_0 = 1500$ m/s, $c_1 = 1350$ m/s and $c_2 = 1500$ m/s, and there is no critical reflection. The depths of the two interfaces in both examples are $z_a = 1000$ m and $z_b = 1075$ m.

The data are synthesized in the τ-p domain and so can be considered to have been generated from an experiment with infinite spatial aperture. Figure 5 shows the reflectivity data for the two models. In both cases, the minimum and maximum source frequencies are $f_{min} = 0.25$ Hz and $f_{max} = 62.5$ Hz, respectively. We choose to display the result as "spike-like" data, rather than "box-like" α_1, by taking the derivative of the result with respect to z. This is done primarily because it is easier to detect the shifting of reflectors when displayed in "spike-like" form. Figure 6 shows the results of imaging the data in Fig. 5 using the constant reference velocity, c_0. The mislocated reflector exhibits residual moveout when imaged with the first term in the series (left). The leading order imaging series (right) improves the depth at all angles and acts to "flatten" the imaged reflector. As expected from the leading order approximation, a small amount of residual moveout remains.

Figure 7 compares the result of summing eight terms in the leading order imaging series (21) with the closed form result (24). After summing eight terms, the series has converged and the deeper reflector has been relocated to the depth predicted analytically. Summing more terms in the leading order imaging series does not further correct the depth because the terms are too small. Differences in appearance between the series summation and the closed form result can be attributed to the artifacts associated with the numerical computation of derivatives.

Figure 8 shows the velocity profile and synthetic data for a 6-layer model. The imaging results using a constant reference velocity are compared in Fig. 9. The leading order imaging series improves the location of all the reflectors mislocated by the first term. The remaining errors in the predicted depths are left to be corrected by higher order imaging terms. A small cumulative error in depth noticeable in Fig. 9 is attributed primarily to the fact the integral of the data in the overburden necessarily includes transmission coefficients that introduce small errors in the series for the shifts.

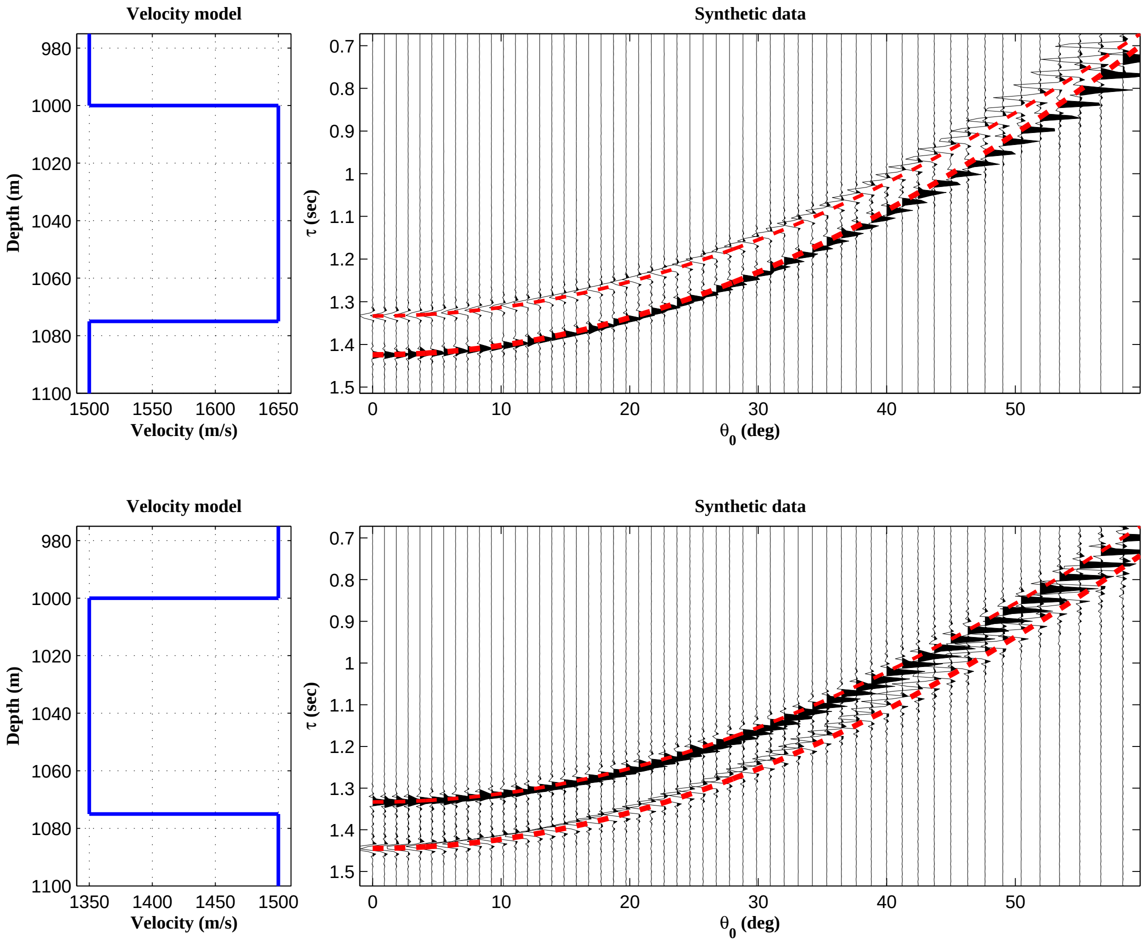

Figure 5: *Velocity model and synthetic reflectivity data in the τ-p domain for two specific two-interface examples. The time derivatives of the data are displayed and the polarity is consistent with the wave equation in (1). The red lines overlying the seismic data are the analytically computed τ values for each reflector.*

4 Discussion

The analytic and numerical results of the prestack leading order imaging series have highlighted a number of interesting characteristics of the algorithm. Given a choice of how to handle the degree of freedom afforded by the source-receiver offset in the seismic experiment, we chose in this paper to keep the angle of incidence in the reference medium (θ_0 or p_0) constant and let ω vary. This allowed for a straightforward generalization of the normal incidence case to non-normal incidence. By parameterizing the problem for a constant θ_0, one can consider a new effective perturbation that is scaled by $1/\cos^2\theta_0$:

$$\frac{\omega^2}{c^2(z)} = \frac{\omega^2}{c_0^2}\left(1-\alpha\left(z\right)\right) = \frac{k_z^2}{\cos^2\theta_0}\left(1-\alpha\left(z\right)\right). \tag{36}$$

For the acoustic examples considered here, the first term in the imaging series more accu-

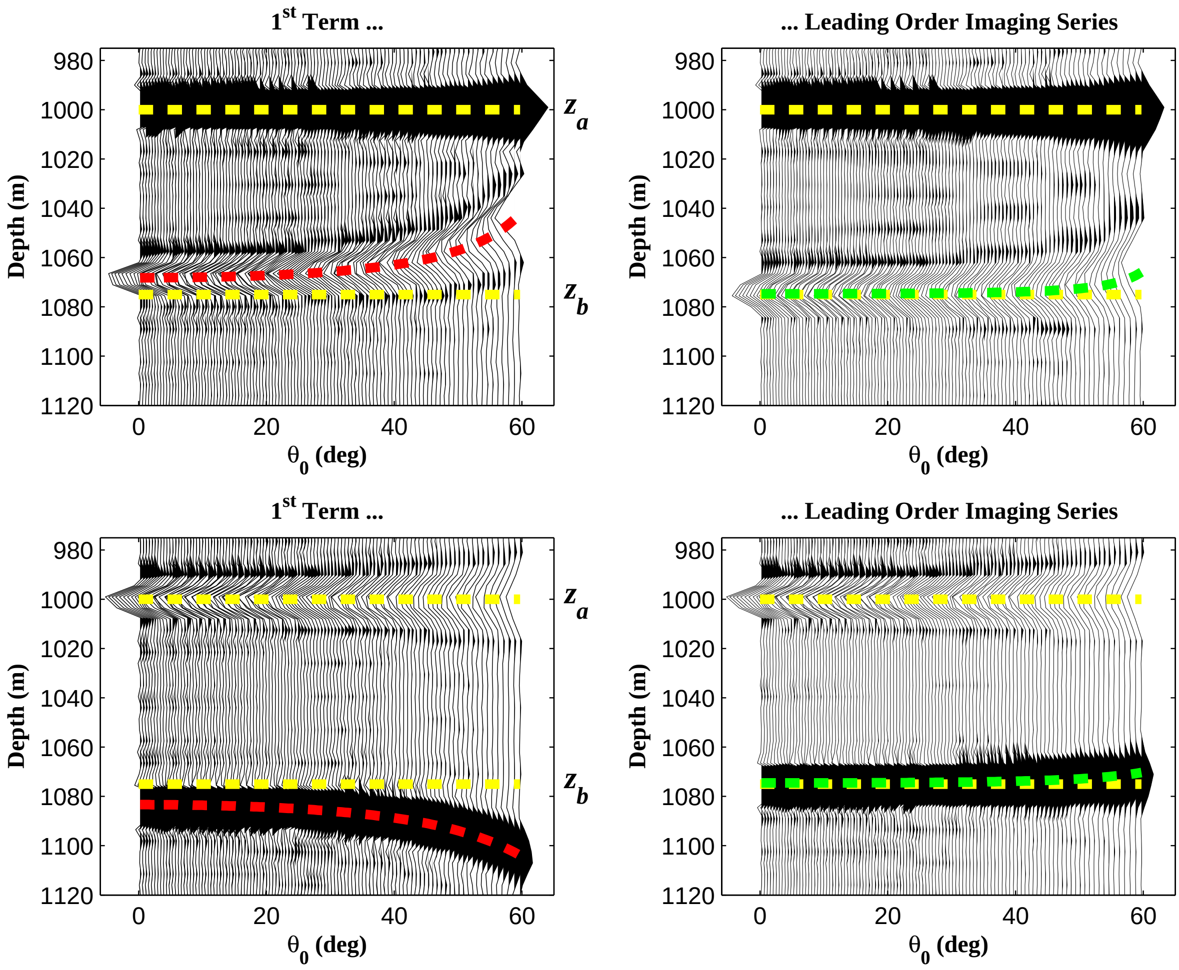

Figure 6: *Results of imaging the two datasets in Fig. 5. At top is the example where the velocity increased, and at bottom is the example where the velocity decreased. On the left is the first term in the series: the result of an imaging algorithm that is linear in the data. On the right is the result of the leading order imaging series. The derivatives with respect to depth of* α^{LOIM} *are displayed. The yellow lines are the actual depths of the two reflectors. The red and green lines are the predicted depths computed analytically using (30) and (34), respectively.*

rately locates reflectors at small angles θ_0. This is because the decomposed plane waves at larger angles spend proportionally longer times in the layers with the wrong velocity. At the same time, the magnitude of the amplitudes at larger angles is greater, which assist the non-linear terms of the leading order imaging series in shifting the reflectors the required distance to their actual locations. This larger "effective contrast" at higher angles also tends to emphasize the fact that the imaging algorithm currently being tested is leading order in the data's amplitudes. This leading order approximation is better at small angles and is it's the reason why the leading order imaging series leaves a small amount of residual moveout. Higher order terms may be required by larger angles of incidence. On the other hand, the

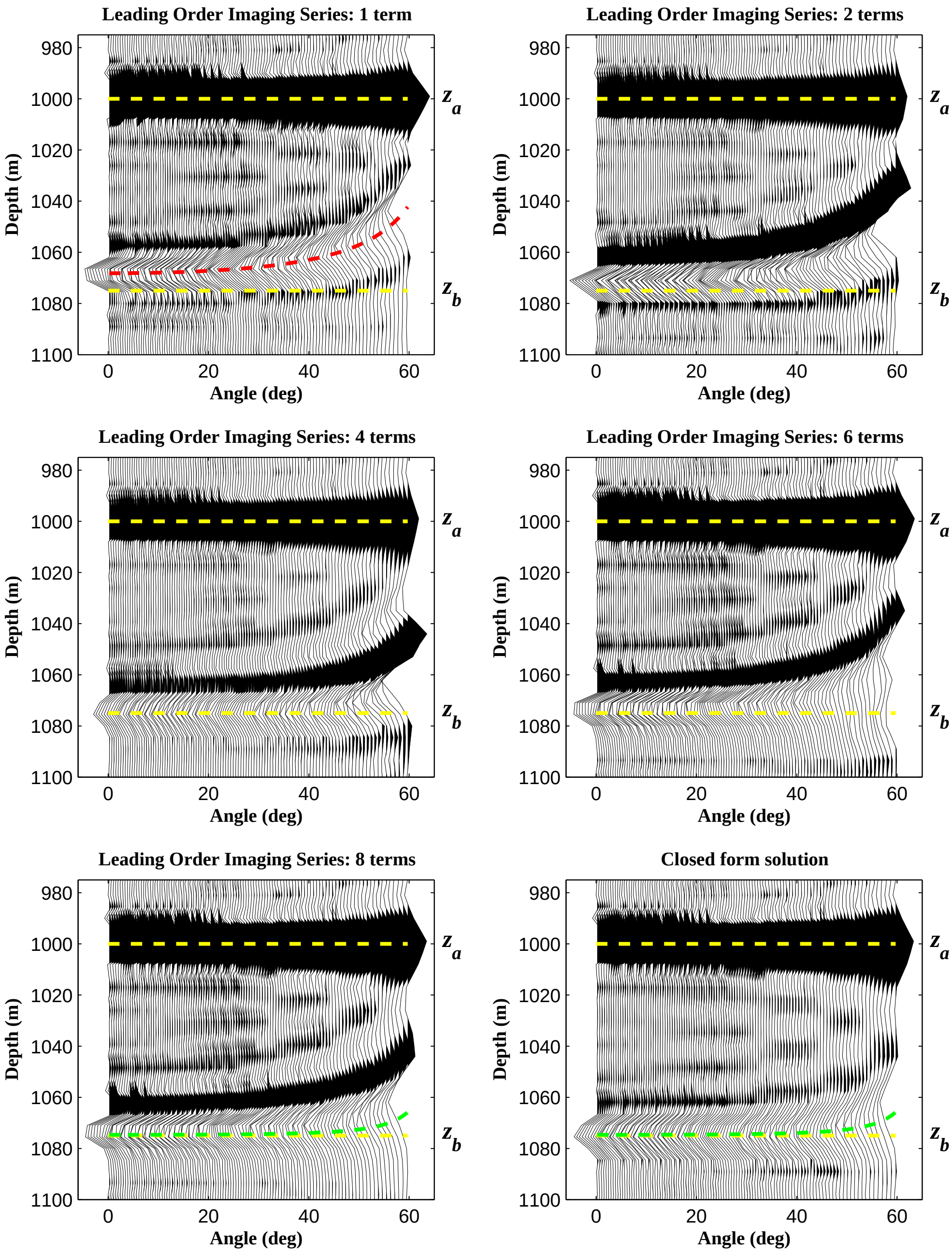

Figure 7: *The cumulative sum of up to eight terms in the leading order imaging series compared to the closed form result. The input data are the same as in Fig. 5 (top) where the reference velocity is slower than the actual velocity in the layer. The red and green lines are the predicted depths computed analytically for the first term and the closed form, respectively.*

rate of convergence of the series form of the algorithm will benefit from the fact that the maximum k_z is smaller at large angles (since $k_z = k_0 \cos\theta_0$).

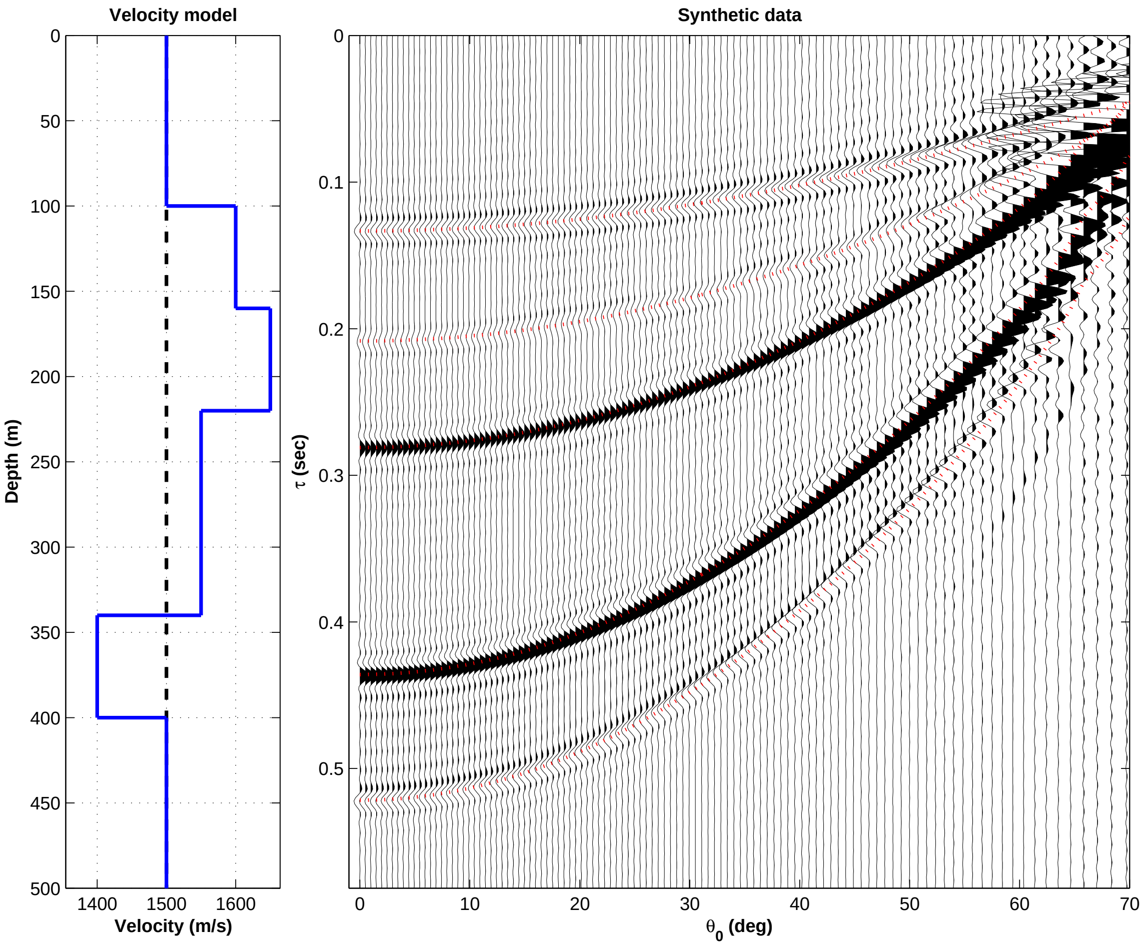

Figure 8: *Velocity profile and synthetic reflectivity data in the τ-p domain for a 6 layer model. The time derivatives of the data are displayed. The red lines overlying the seismic data are the analytically computed τ values for each reflector.*

The reflectivity data that was the input to the numerical tests, was modelled for a source absent of zero frequency. This is itself an important result since field data are always bandlimited. A more detailed analysis of the issues surrounding missing low frequency and the leading order imaging series is given in Part II (Shaw and Weglein, 2004).

5 Conclusion

A prestack formulation of a leading order imaging series for constant angles of incidence and a 1D medium has been derived and analyzed for several analytic and synthetic numerical experiments. The results illustrate the improvement in the predicted depths of the reflectors that are mislocated by conventional depth imaging (which corresponds to the first term in

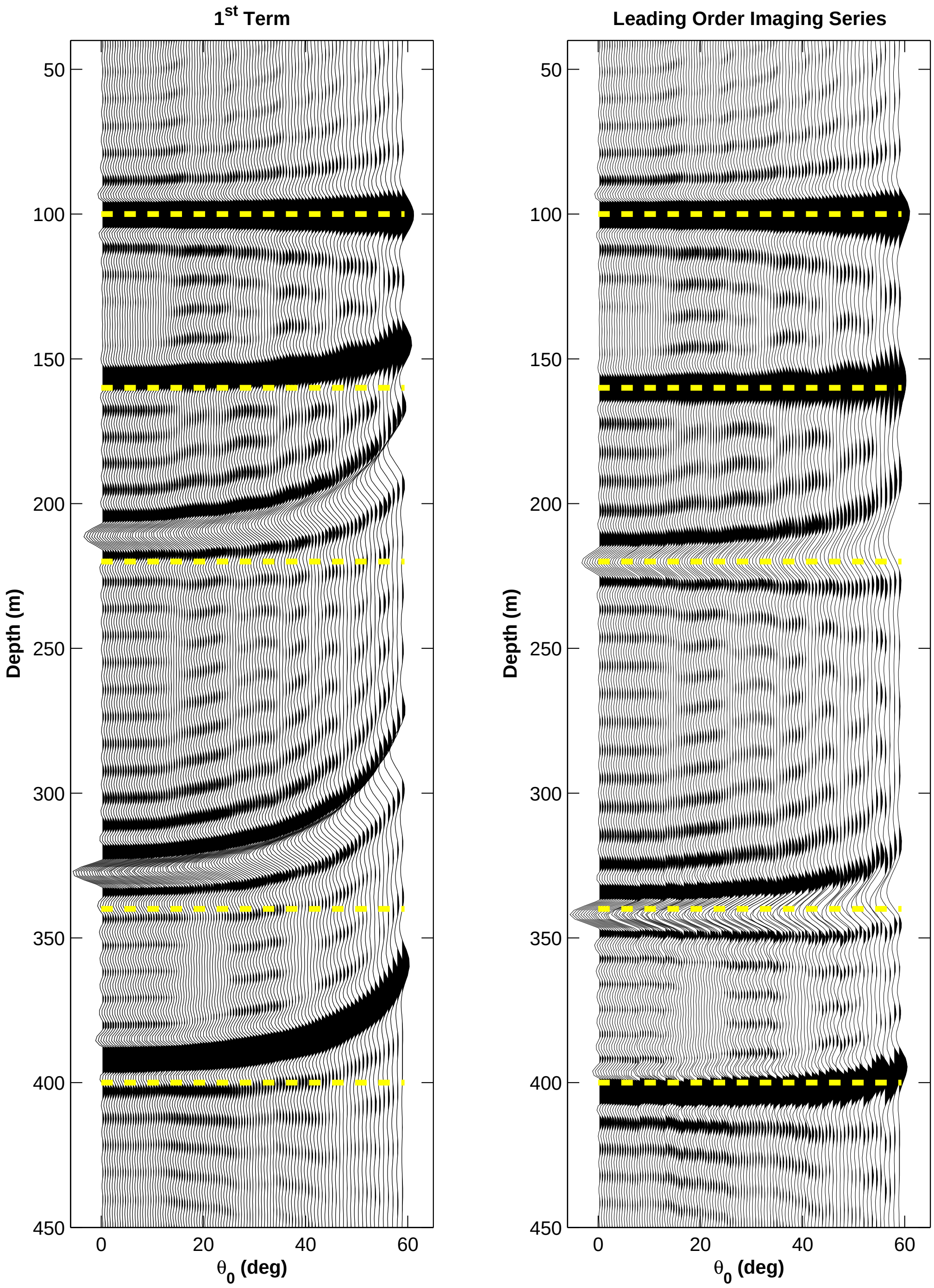

Figure 9: *Results of imaging the data in Fig. 8. On the left is the first term in the series: the result of an imaging algorithm that is linear in the data. On the right is the result of the leading order imaging series. The yellow lines are the actual depths of the reflectors.*

the series). The effect of the leading order imaging series can be visualized as correcting the residual moveout of common image gathers that are imaged with the wrong velocity.

Acknowledgements

ConocoPhillips (especially Hugh Rowlett and Rob Habiger) are thanked for their financial support (of S. A. Shaw) and for their encouragement of this research. Ken Matson and Gerhard Pfau at BP are thanked for releasing the reflectivity code and we are grateful to Dennis Corrigan for his support of that code. Einar Otnes, Kris Innanen and Bogdan Nita are thanked for their excellent suggestions that improved this manuscript. We are grateful to the sponsors of M-OSRP for supporting this project.

References

Carvalho, P. M. (1992). *Free-surface multiple reflection elimination method based on non-linear inversion of seismic data.* Ph. D. thesis, Universidade Federal da Bahia.

DeSanto, J. A. (1992). *Scalar Wave Theory: Green's Functions and Applications.* Springer-Verlag.

Innanen, K. A. (2003). High/low order imaging terms? Personal Communication.

Jacobs, B. (1980). A program for inversion by T-matrix iteration. *Stanford Exploration Project 24.*

Kennett, B. L. N. (1983). *Seismic Wave Propagation in Stratified Media* (2nd ed.). Cambridge University Press.

Liu, F., B. G. Nita, A. B. Weglein, and K. A. Innanen (2004). Inverse scattering series in the presence of lateral variations. *M-OSRP Annual Report 3.*

Moses, H. (1956). Calculation of scattering potential from reflection coefficients. *Phys. Rev.* (102), 559–567.

Razavy, M. (1975). Determination of the wave velocity in an inhomogeneous medium from reflection data. *J. Acoust. Soc. Am. 58*, 956–963.

Shaw, S. A. and A. B. Weglein (2004). A leading order imaging series for prestack data acquired over a laterally invariant acoustic medium. Part II: Analysis for data missing low frequencies. *M-OSRP Annual Report 3.*

Shaw, S. A., A. B. Weglein, D. J. Foster, K. H. Matson, and R. G. Keys (2003). Isolation of a leading order depth imaging series and analysis of its convergence properties. *M-OSRP Annual Report 2*, 157–195.

Stolt, R. H. and B. Jacobs (1980). Inversion of seismic data in a laterally heterogeneous medium. *Stanford Exploration Project 24*.

Treitel, S., P. R. Gutowski, and D. E. Wagner (1982). Plane-wave decomposition of seismograms. *Geophysics 47*(10), 1375–1401.

Weglein, A. B., F. V. Araújo, P. M. Carvalho, R. H. Stolt, K. H. Matson, R. T. Coates, D. Corrigan, D. J. Foster, S. A. Shaw, and H. Zhang (2003). Inverse scattering series and seismic exploration. *Inverse Problems 19*, R27–R83.

Weglein, A. B., W. E. Boyce, and J. E. Anderson (1981). Obtaining three-dimensional velocity information directly from reflection seismic data: An inverse scattering formalism. *Geophysics 46*(8), 1116–1120.

Weglein, A. B., D. J. Foster, K. H. Matson, S. A. Shaw, P. M. Carvalho, and D. Corrigan (2002). Predicting the correct spatial location of reflectors without knowing or determining the precise medium and wave velocity: initial concept, algorithm and analytic and numerical example. *Journal of Seismic Exploration 10*, 367–382.

Weglein, A. B., F. A. Gasparotto, P. M. Carvalho, and R. H. Stolt (1997). An inverse-scattering series method for attenuating multiples in seismic reflection data. *Geophysics 62*(6), 1975–1989.

Weglein, A. B., K. H. Matson, D. J. Foster, P. M. Carvalho, D. Corrigan, and S. A. Shaw (2000). Imaging and inversion at depth without a velocity model: Theory, concepts and initial evaluation. In *70th Annual Internat. Mtg., Soc. Expl. Geophys., Expanded Abstracts*, pp. 1016–1019. Soc. Expl. Geophys.

Zhang, H. and A. B. Weglein (2004). Target identification using the inverse scattering series: data requirements for the direct inversion of large-contrast, inhomogeneous elastic media. *M-OSRP Annual Report 3*.

A Derivation of the first term, α_1

The first term in the inverse series is a linear inversion of the scattered field. Beginning with (5), the data $\tilde{D}$ are related to α_1 by

$$\tilde{D}\left(\vec{x}_g|\vec{x}_s;\omega\right) = \int_{-\infty}^{\infty} dx' \int_{-\infty}^{\infty} dy' \int_{-\infty}^{\infty} dz' G_0\left(\vec{x}_g|\vec{x}\,';\omega\right) k_0^2 \alpha_1\left(\vec{x}\,'\right) G_0\left(\vec{x}\,'|\vec{x}_s;\omega\right) \tag{37}$$

where $k_0 = \omega/c_0$. The two reference Green's functions in (37) satisfy

$$\left(\nabla^2 + \frac{\omega^2}{c_0^2}\right) G_0 = -\delta \tag{38}$$

and the causal solutions are (see, for example, DeSanto (1992))

$$G_0(\vec{x}_g|\vec{x}\,';\omega)=\frac{1}{(2\pi)^3}\int_{-\infty}^{\infty}dk_{x'}\int_{-\infty}^{\infty}dk_{y'}\int_{-\infty}^{\infty}dk_{z'}\frac{e^{ik_{x'}(x_g-x')}e^{ik_{y'}(y_g-y')}e^{ik_{z'}(z_g-z')}}{k_0^2-k_{x'}^2-k_{y'}^2-k_{z'}^2} \tag{39}$$

$$G_0(\vec{x}\,'|\vec{x}_s;\omega)=\frac{1}{(2\pi)^3}\int_{-\infty}^{\infty}dk_{x_s}\int_{-\infty}^{\infty}dk_{y_s}\int_{-\infty}^{\infty}dk_{z_s}\frac{e^{ik_{x_s}(x'-x_s)}e^{ik_{y_s}(y'-y_s)}e^{ik_{z_s}(z'-z_s)}}{k_0^2-k_{x_s}^2-k_{y_s}^2-k_{z_s}^2}. \tag{40}$$

Implicit in (37) is that the incident field is the result of a point source and not a plane wave. Substituting these Green's functions into (37) yields

$$\begin{aligned}\tilde{D}\left(\vec{x}_g|\vec{x}_s;\omega\right)=&\frac{1}{(2\pi)^6}\int_{-\infty}^{\infty}dx'\int_{-\infty}^{\infty}dy'\int_{-\infty}^{\infty}dz'\int_{-\infty}^{\infty}dk_{x'}\int_{-\infty}^{\infty}dk_{y'}\\&\times\int_{-\infty}^{\infty}dk_{z'}\frac{e^{ik_{x'}(x_g-x')}e^{ik_{y'}(y_g-y')}e^{ik_{z'}(z_g-z')}}{k_0^2-k_{x'}^2-k_{y'}^2-k_{z'}^2}k_0^2\alpha_1(\vec{x}\,')\\&\times\int_{-\infty}^{\infty}dk_{x_s}\int_{-\infty}^{\infty}dk_{y_s}\int_{-\infty}^{\infty}dk_{z_s}\frac{e^{ik_{x_s}(x'-x_s)}e^{ik_{y_s}(y'-y_s)}e^{ik_{z_s}(z'-z_s)}}{k_0^2-k_{x_s}^2-k_{y_s}^2-k_{z_s}^2}.\end{aligned} \tag{41}$$

Performing a double Fourier transform over x_g and y_g

$$\begin{aligned}\tilde{D}(k_{x_g},k_{y_g},z_g|\vec{x}_s;\omega)=&\int_{-\infty}^{\infty}dx_g\int_{-\infty}^{\infty}dy_g\tilde{D}\left(x_g,y_g,z_g|\vec{x}_s;\omega\right)e^{-ik_{x_g}x_g}e^{-ik_{y_g}y_g}\\=&\frac{1}{(2\pi)^6}\underbrace{\int_{-\infty}^{\infty}dx_g\int_{-\infty}^{\infty}dy_g}\int_{-\infty}^{\infty}dx'\int_{-\infty}^{\infty}dy'\int_{-\infty}^{\infty}dz'\\&\times\int_{-\infty}^{\infty}dk_{x'}\int_{-\infty}^{\infty}dk_{y'}\underbrace{e^{ix_g(k_{x'}-k_{x_g})}e^{iy_g(k_{y'}-k_{y_g})}}\\&\times\int_{-\infty}^{\infty}dk_{z'}\frac{e^{-ik_{x'}x'}e^{-ik_{y'}y'}e^{ik_{z'}(z_g-z')}}{k_0^2-k_{x'}^2-k_{y'}^2-k_{z'}^2}\\\times k_0^2\alpha_1(\vec{x}\,')&\int_{-\infty}^{\infty}dk_{x_s}\int_{-\infty}^{\infty}dk_{y_s}\int_{-\infty}^{\infty}dk_{z_s}\frac{e^{ik_{x_s}(x'-x_s)}e^{ik_{y_s}(y'-y_s)}e^{ik_{z_s}(z'-z_s)}}{k_0^2-k_{x_s}^2-k_{y_s}^2-k_{z_s}^2}.\end{aligned} \tag{42}$$

Carrying out the integrations over x_g and y_g (braced terms) produces two delta functions $(2\pi)^2\delta(k_{x'}-k_{x_g})\delta(k_{y'}-k_{y_g})$. Then the integrations over $k_{x'}$ and $k_{y'}$ can be performed giving

$$\begin{aligned}\tilde{D}(k_{x_g},k_{y_g},z_g|\vec{x}_s;\omega)=&\frac{1}{(2\pi)^4}\int_{-\infty}^{\infty}dx'\int_{-\infty}^{\infty}dy'\int_{-\infty}^{\infty}dz'\\&\times\int_{-\infty}^{\infty}dk_{z'}\frac{e^{-ik_{x_g}x'}e^{-ik_{y_g}y'}e^{ik_{z'}(z_g-z')}}{k_0^2-k_{x_g}^2-k_{y_g}^2-k_{z'}^2}k_0^2\alpha_1(\vec{x}\,')\\\times&\int_{-\infty}^{\infty}dk_{x_s}\int_{-\infty}^{\infty}dk_{y_s}\int_{-\infty}^{\infty}dk_{z_s}\frac{e^{ik_{x_s}(x'-x_s)}e^{ik_{y_s}(y'-y_s)}e^{ik_{z_s}(z'-z_s)}}{k_0^2-k_{x_s}^2-k_{y_s}^2-k_{z_s}^2}\end{aligned} \tag{43}$$

Now assume that the actual medium is invariant in the x and y directions, i.e.,

$$\alpha_1(\vec{x}) = \alpha_1(z). \tag{44}$$

Collecting the exponentials in x' and y' and then carrying out the integrations over these variable produces two more delta functions (braced terms below) allowing integration over k_{x_s} and k_{y_s}:

$$\begin{aligned}
\tilde{D}(k_{x_g}, k_{y_g}, z_g|\vec{x}_s;\omega) =& \frac{1}{(2\pi)^4} \underbrace{\int_{-\infty}^{\infty} dx' \int_{-\infty}^{\infty} dy'} \int_{-\infty}^{\infty} dz' \int_{-\infty}^{\infty} dk_{z'} \\
& \times \frac{e^{ik_{z'}(z_g - z')}}{k_0^2 - k_{x_g}^2 - k_{y_g}^2 - k_{z'}^2} k_0^2 \alpha_1(z') \\
& \times \int_{-\infty}^{\infty} dk_{x_s} \underbrace{e^{ix'(k_{x_s} - k_{x_g})}} \int_{-\infty}^{\infty} dk_{y_s} \underbrace{e^{iy'(k_{y_s} - k_{y_g})}} \\
& \times \int_{-\infty}^{\infty} dk_{z_s} \frac{e^{-ik_{x_s}x_s} e^{-ik_{y_s}y_s} e^{ik_{z_s}(z' - z_s)}}{k_0^2 - k_{x_s}^2 - k_{y_s}^2 - k_{z_s}^2} \\
=& \frac{1}{(2\pi)^2} \int_{-\infty}^{\infty} dz' \int_{-\infty}^{\infty} dk_{z'} \frac{e^{ik_{z'}(z_g - z')}}{k_0^2 - k_{x_g}^2 - k_{y_g}^2 - k_{z'}^2} \\
& \times k_0^2 \alpha_1(z') \int_{-\infty}^{\infty} dk_{z_s} \frac{e^{-ik_{x_g}x_s} e^{-ik_{y_g}y_s} e^{ik_{z_s}(z' - z_s)}}{k_0^2 - k_{x_g}^2 - k_{y_g}^2 - k_{z_s}^2}.
\end{aligned} \tag{45}$$

Note that the integrations over x' and y' in (45), for a laterally invariant medium where α_1 is not a function of x' or y', demonstrates that $k_{x_g} = k_{x_s}$ and $k_{y_g} = k_{y_s}$. Define the vertical wavenumbers

$$q_g^2 = k_0^2 - k_{x_g}^2 - k_{y_g}^2 \tag{46}$$

and

$$q_s^2 = k_0^2 - k_{x_s}^2 - k_{y_s}^2 \tag{47}$$

which, for the case where α is only a function of z, are equal ($q_g = q_s$). Substituting (46) into (45),

$$\begin{aligned}
\tilde{D}(k_{x_g}, k_{y_g}, z_g|\vec{x}_s;\omega) =& \frac{1}{(2\pi)^2} e^{-ik_{x_g}x_s} e^{-ik_{y_g}y_s} \int_{-\infty}^{\infty} dz' k_0^2 \alpha_1(z') \\
& \times \int_{-\infty}^{\infty} dk_{z'} \frac{e^{ik_{z'}(z_g - z')}}{q_g^2 - k_{z'}^2} \int_{-\infty}^{\infty} dk_{z_s} \frac{e^{ik_{z_s}(z' - z_s)}}{q_g^2 - k_{z_s}^2}.
\end{aligned} \tag{48}$$

We are now in a position to perform the integrals with respect to $k_{z'}$ and k_{z_s} (see, e.g., DeSanto (1992), page 57):

$$\begin{aligned}
\int_{-\infty}^{\infty} dk_{z'} \frac{e^{ik_{z'}(z_g - z')}}{q_g^2 - k_{z'}^2} &= - \int_{-\infty}^{\infty} dk_{z'} \frac{e^{ik_{z'}(z_g - z')}}{(k_{z'} - q_g)(k_{z'} + q_g)} \\
&= -\frac{\pi i}{q_g} e^{iq_g|z_g - z'|}
\end{aligned} \tag{49}$$

and similarly

$$\int_{-\infty}^{\infty} dk_{z_s} \frac{e^{ik_{z_s}(z'-z_s)}}{q_g^2 - k_{z_s}^2} = -\frac{\pi i}{q_g} e^{iq_g|z'-z_s|}. \tag{50}$$

Substituting (49) and (50) into (48) gives

$$\begin{aligned}
\tilde{D}(k_{x_g}, k_{y_g}, z_g|\vec{x}_s;\omega) =& \frac{1}{(2\pi)^2} e^{-ik_{x_g}x_s} e^{-ik_{y_g}y_s} \int_{-\infty}^{\infty} dz' k_0^2 \alpha_1(z') \left(-\frac{\pi i}{q_g} e^{iq_g|z_g-z'|}\right)\left(-\frac{\pi i}{q_g} e^{iq_g|z'-z_s|}\right) \\
=& \frac{e^{-ik_{x_g}x_s} e^{-ik_{y_g}y_s}}{-4q_g^2} \int_{-\infty}^{\infty} dz' e^{iq_g(z'-z_g)} k_0^2 \alpha_1(z') e^{iq_g(z'-z_s)} \\
=& \frac{k_0^2}{-4q_g^2} e^{-ik_{x_g}x_s} e^{-ik_{y_g}y_s} e^{-iq_g(z_g+z_s)} \tilde{\alpha}_1(-2q_g)
\end{aligned} \tag{51}$$

where in (51) we have assumed that the scattering points are below the measurement surface ($z' > z_g$ and $z' > z_s$). Performing a double inverse Fourier transform

$$\begin{aligned}
\tilde{D}(\vec{x}_g|\vec{x}_s;\omega) =& \frac{1}{(2\pi)^2} \int_{-\infty}^{\infty} dk_{x_g} e^{ik_{x_g}x_g} \int_{-\infty}^{\infty} dk_{y_g} e^{ik_{y_g}y_g} \tilde{D}(k_{x_g}, k_{y_g}, z_g|\vec{x}_s;\omega) \\
=& \frac{1}{(2\pi)^2} \int_{-\infty}^{\infty} dk_{x_g} e^{ik_{x_g}x_g} \int_{-\infty}^{\infty} dk_{y_g} e^{ik_{y_g}y_g} \frac{k_0^2}{-4q_g^2} e^{-ik_{x_g}x_s} e^{-ik_{y_g}y_s} e^{-iq_g(z_g+z_s)} \tilde{\alpha}_1(-2q_g) \\
=& \frac{1}{(2\pi)^2} \int_{-\infty}^{\infty} dk_{x_g} \int_{-\infty}^{\infty} dk_{y_g} \frac{k_0^2}{-4q_g^2} \tilde{\alpha}_1(-2q_g) e^{ik_{x_g}(x_g-x_s)} e^{ik_{y_g}(y_g-y_s)} e^{-iq_g(z_g+z_s)}.
\end{aligned} \tag{52}$$

We proceed by changing from cartesian to cylindrical coordinates where

$$\int_{-\infty}^{\infty} dk_{x_g} \int_{-\infty}^{\infty} dk_{y_g} = \int_0^{\infty} k_r dk_r \int_0^{2\pi} d\tilde{\phi}. \tag{53}$$

Substituting (53) into (52) yields

$$\tilde{D}(r, z;\omega) = \frac{1}{(2\pi)^2} \int_0^{\infty} dk_r \int_0^{2\pi} d\tilde{\phi} \frac{k_0^2 k_r}{-4q_g^2} \tilde{\alpha}_1(-2q_g) e^{ik_r \cos\tilde{\phi} r \cos\phi} e^{ik_r \sin\tilde{\phi} r \sin\phi} e^{-iq_g(z_g+z_s)} \tag{54}$$

and, since,

$$\int_0^{2\pi} e^{ik_r r\left(\cos\tilde{\phi}\cos\phi + \sin\tilde{\phi}\sin\phi\right)} d\tilde{\phi} = \int_0^{2\pi} e^{ik_r r\left(\cos\left(\tilde{\phi}-\phi\right)\right)} d\tilde{\phi} = 2\pi J_0(k_r r), \tag{55}$$

then (54) becomes

$$\tilde{D}(r;\omega) = \frac{1}{(2\pi)} \int_0^{\infty} \frac{k_0^2}{-4q_g^2} \tilde{\alpha}_1(-2q_g) e^{-iq_g(z_g+z_s)} J_0(k_r r) k_r dk_r \tag{56}$$

which is an expression for the scattered field in terms of $\tilde{\alpha}_1$. Equation (56) can be inverted by recognizing the Fourier-Bessel transform pairs

$$g(r) = \int_0^\infty G(k_r) J_0(k_r r) k_r dk_r \tag{57}$$

$$G(k_r) = \int_0^\infty g(r) J_0(k_r r) r dr \tag{58}$$

and leads to

$$\frac{1}{(2\pi)} \frac{k_0^2}{-4q_g^2} \tilde{\alpha}_1(-2q_g) e^{-iq_g(z_g+z_s)} = \int_0^\infty \tilde{D}(r;\omega) J_0(k_r r) r dr. \tag{59}$$

Therefore,

$$\tilde{\alpha}_1(-2q_g) = 2\pi \frac{-4q_g^2}{k_0^2} e^{iq_g(z_g+z_s)} \int_0^\infty \tilde{D}(r;\omega) J_0(k_r r) r dr. \tag{60}$$

where

$$q_g = \frac{\omega}{c_0} \sqrt{1 - \frac{k_r^2 c_0^2}{\omega^2}}. \tag{61}$$

From (60), we see that $\tilde{\alpha}_1$ is over-determined (there are more free variables on the right-hand side than on the left). Inverse Fourier transforming both sides of (60) gives

$$\begin{aligned} \alpha_1(z) =& \frac{2}{2\pi} \int_{-\infty}^\infty \tilde{\alpha}_1(-2q_g) e^{-2iq_g z} dq_g \\ =& -8 \int_{-\infty}^\infty \frac{q_g^2}{k_0^2} e^{-iq_g(2z-(z_g+z_s))} \int_0^\infty \tilde{D}(r;\omega) J_0(k_r r) r dr dq_g \end{aligned} \tag{62}$$

Considering fixed angles of incidence, θ_0, leads to a number of different estimates of α_1, denoted by $\alpha_1(z,\theta_0)$. Fixing θ_0 is the same as fixing horizontal and vertical slownesses, $p = p_0$ and $\zeta = \zeta_0$, respectively, where

$$p_0 = \frac{\sin\theta_0}{c_0} \text{ and } \zeta_0 = \frac{\cos\theta_0}{c_0}.$$

However, q_g is still allowed to vary through the variation in ω (since $q_g = \omega\zeta_0$). We proceed by changing variables from q_g to ω:

$$\alpha_1(z,\theta_0) = -8\zeta_0 \cos^2\theta_0 \int_{-\infty}^\infty e^{-i\omega\zeta_0(2z-(z_g+z_s))} \int_0^\infty \tilde{D}(r;\omega) J_0(\omega p_0 r) r dr d\omega \tag{63}$$

Define $\tau_0 = \zeta_0 \left(2z - (z_g + z_s)\right)$ and substitute (a) the temporal Fourier transform of the data $D(r,t)$ for $\widetilde{D}(r;\omega)$ and (b) the integral form of the Bessel function gives

$$\begin{aligned}
\alpha_1(z,\theta_0) =& -8\zeta_0 \cos^2\theta_0 \int_{-\infty}^{\infty} d\omega e^{-i\omega\tau_0} \int_0^{\infty} rdr \left(\int_{-\infty}^{\infty} D(r;t)e^{i\omega t}dt\right)\left(\frac{1}{2\pi}\int_0^{2\pi} e^{i\omega p_0 r\cos\phi}d\phi\right) \\
=& -8\zeta_0 \cos^2\theta_0 \int_{-\infty}^{\infty} d\omega \int_0^{\infty} rdr \left(\int_{-\infty}^{\infty} D(r;t)e^{i\omega(t-(\tau_0-p_0 r\cos\phi))}dt\right)\left(\frac{1}{2\pi}\int_0^{2\pi} d\phi\right) \\
=& -8\zeta_0 \cos^2\theta_0 \int_0^{\infty} rdr \left(\int_{-\infty}^{\infty} D(r;t)2\pi\delta(t-(\tau_0-p_0 r\cos\phi))dt\right) \\
=& -8\zeta_0 \cos^2\theta_0 \int_0^{2\pi}\int_0^{\infty} D(r;\tau_0-p_0 r\cos\phi)rdrd\phi
\end{aligned} \tag{64}$$

Changing back to cartesian coordinates, where

$$r = \sqrt{x^2+y^2}, \quad \phi = \arccos\left(\frac{x}{\sqrt{x^2+y^2}}\right), \quad \phi = \arcsin\left(\frac{y}{\sqrt{x^2+y^2}}\right)$$

and the partial derivatives are

$$\begin{aligned}
\frac{\partial r}{\partial x} &= \frac{x}{\sqrt{x^2+y^2}} = \frac{x}{r} \\
\frac{\partial r}{\partial y} &= \frac{y}{\sqrt{x^2+y^2}} = \frac{y}{r} \\
\frac{\partial \phi}{\partial x} &= \frac{-1}{\sqrt{1-\left(\frac{x}{\sqrt{x^2+y^2}}\right)^2}} \times \frac{\left(\sqrt{x^2+y^2} - \frac{x^2}{\sqrt{x^2+y^2}}\right)}{(x^2+y^2)} \\
&= \frac{\left(\frac{x^2}{r} - r\right)}{r^2\sqrt{1-\left(\frac{x^2}{r^2}\right)}} = \frac{\frac{1}{r}\left(x^2-r^2\right)}{r\sqrt{r^2-x^2}} = \frac{-y}{r^2}
\end{aligned}$$

$$\begin{aligned}
\frac{\partial \phi}{\partial y} &= \frac{1}{\sqrt{1-\left(\frac{y}{\sqrt{x^2+y^2}}\right)^2}} \times \frac{\left(\sqrt{x^2+y^2} - \frac{y^2}{\sqrt{x^2+y^2}}\right)}{(x^2+y^2)} \\
&= \frac{\left(r - \frac{y^2}{r}\right)}{r^2\sqrt{1-\left(\frac{y^2}{r^2}\right)}} = \frac{\frac{1}{r}\left(r^2-y^2\right)}{r\sqrt{r^2-y^2}} = \frac{x}{r^2}.
\end{aligned}$$

So the Jacobian is

$$\frac{\partial r}{\partial x}\frac{\partial \phi}{\partial y} - \frac{\partial r}{\partial y}\frac{\partial \phi}{\partial x} = \frac{x^2}{r^3} + \frac{y^2}{r^3} = \frac{1}{r}$$

and therefore

$$\alpha_1(z,\theta_0) = -8\zeta_0 \cos^2\theta_0 \int_{-\infty}^{\infty}\int_{-\infty}^{\infty} D(x,y;\tau_0 - xp_0)dxdy \tag{65}$$

where $\tau_0 = \zeta_0\left(2z - (z_g + z_s)\right)$ and $p_0 = \sin\theta_0/c_0$. Equation (65) is recognizable as the slant stack of the recorded data (Treitel et al., 1982).

B Derivation of the second term, α_2

The integral equation for the second term in the inverse series for this acoustic problem is

$$\begin{aligned}
&\int_{-\infty}^{\infty} G_0\left(\vec{x}_g|\vec{x}';\omega\right)k_0^2\alpha_2(\vec{x}')G_0\left(\vec{x}'|\vec{x}_s;\omega\right)d\vec{x}' \\
&\qquad = -\int_{-\infty}^{\infty} d\vec{x}'\, G_0\left(\vec{x}_g|\vec{x}';\omega\right)k_0^2\alpha_1(\vec{x}') \\
&\qquad\quad \times \int_{-\infty}^{\infty} d\vec{x}''\, G_0\left(\vec{x}'|\vec{x}'';\omega\right)k_0^2\alpha_1(\vec{x}'')G_0\left(\vec{x}''|\vec{x}_s;\omega\right).
\end{aligned}\tag{66}$$

Upon substitution of the causal Green's functions, the left-hand side becomes

$$\begin{aligned}
LHS =& \frac{1}{(2\pi)^6}\int_{-\infty}^{\infty}dx'\int_{-\infty}^{\infty}dy'\int_{-\infty}^{\infty}dz' \\
&\times \int_{-\infty}^{\infty}dk_{x'}\int_{-\infty}^{\infty}dk_{y'}\int_{-\infty}^{\infty}dk_{z'}\frac{e^{ik_{x'}(x_g-x')}e^{ik_{y'}(y_g-y')}e^{ik_{z'}(z_g-z')}}{k_0^2-k_{x'}^2-k_{y'}^2-k_{z'}^2} \\
&\times k_0^2\alpha_2(z')\int_{-\infty}^{\infty}dk_{x_s}\int_{-\infty}^{\infty}dk_{y_s}\int_{-\infty}^{\infty}dk_{z_s}\frac{e^{ik_{x_s}(x'-x_s)}e^{ik_{y_s}(y'-y_s)}e^{ik_{z_s}(z'-z_s)}}{k_0^2-k_{x_s}^2-k_{y_s}^2-k_{z_s}^2}
\end{aligned}\tag{67}$$

and the right-hand side is

$$\begin{aligned}
RHS =& \frac{-1}{(2\pi)^9}\int_{-\infty}^{\infty}dx'\int_{-\infty}^{\infty}dy'\int_{-\infty}^{\infty}dz' \\
&\times \int_{-\infty}^{\infty}dk_{x'}\int_{-\infty}^{\infty}dk_{y'}\int_{-\infty}^{\infty}dk_{z'}\frac{e^{ik_{x'}(x_g-x')}e^{ik_{y'}(y_g-y')}e^{ik_{z'}(z_g-z')}}{k_0^2-k_{x'}^2-k_{y'}^2-k_{z'}^2} \\
&\times k_0^2\alpha_1(z')\int_{-\infty}^{\infty}dx''\int_{-\infty}^{\infty}dy''\int_{-\infty}^{\infty}dz'' \\
&\times \int_{-\infty}^{\infty}dk_{x''}\int_{-\infty}^{\infty}dk_{y''}\int_{-\infty}^{\infty}dk_{z''}\frac{e^{ik_{x''}(x'-x'')}e^{ik_{y''}(y'-y'')}e^{ik_{z''}(z'-z'')}}{k_0^2-k_{x''}^2-k_{y''}^2-k_{z''}^2}k_0^2\alpha_1(z'') \\
&\times \int_{-\infty}^{\infty}dk_{x_s}\int_{-\infty}^{\infty}dk_{y_s}\int_{-\infty}^{\infty}dk_{z_s}\frac{e^{ik_{x_s}(x''-x_s)}e^{ik_{y_s}(y''-y_s)}e^{ik_{z_s}(z''-z_s)}}{k_0^2-k_{x_s}^2-k_{y_s}^2-k_{z_s}^2}.
\end{aligned}\tag{68}$$

As with deriving an equation for α_1, we Fourier transform both sides over x_g and y_g and perform the integrations over $k_{x'}$ and $k_{y'}$. Therefore,

$$\begin{aligned} LHS \to & \frac{1}{(2\pi)^4}\int_{-\infty}^{\infty} dx' \int_{-\infty}^{\infty} dy' \int_{-\infty}^{\infty} dz' \int_{-\infty}^{\infty} dk_{z'} \frac{e^{-ik_{x_g}x'}e^{-ik_{y_g}y'}e^{ik_{z'}(z_g-z')}}{k_0^2-k_{x_g}^2-k_{y_g}^2-k_{z'}^2} \\ & \times k_0^2\alpha_2(z') \int_{-\infty}^{\infty} dk_{x_s} \int_{-\infty}^{\infty} dk_{y_s} \int_{-\infty}^{\infty} dk_{z_s} \frac{e^{ik_{x_s}(x'-x_s)}e^{ik_{y_s}(y'-y_s)}e^{ik_{z_s}(z'-z_s)}}{k_0^2-k_{x_s}^2-k_{y_s}^2-k_{z_s}^2} \end{aligned} \tag{69}$$

$$\begin{aligned} RHS \to & \frac{-1}{(2\pi)^7}\int_{-\infty}^{\infty} dx' \int_{-\infty}^{\infty} dy' \int_{-\infty}^{\infty} dz' \int_{-\infty}^{\infty} dk_{z'} \\ & \times \frac{e^{-ik_{x_g}x'}e^{-ik_{y_g}y'}e^{ik_{z'}(z_g-z')}}{k_0^2-k_{x_g}^2-k_{y_g}^2-k_{z'}^2} k_0^2\alpha_1(z') \int_{-\infty}^{\infty} dx'' \int_{-\infty}^{\infty} dy'' \int_{-\infty}^{\infty} dz'' \\ & \times \int_{-\infty}^{\infty} dk_{x''} \int_{-\infty}^{\infty} dk_{y''} \int_{-\infty}^{\infty} dk_{z''} \\ & \times \frac{e^{ik_{x''}(x'-x'')}e^{ik_{y''}(y'-y'')}e^{ik_{z''}(z'-z'')}}{k_0^2-k_{x''}^2-k_{y''}^2-k_{z''}^2} k_0^2\alpha_1(z'') \\ & \times \int_{-\infty}^{\infty} dk_{x_s} \int_{-\infty}^{\infty} dk_{y_s} \int_{-\infty}^{\infty} dk_{z_s} \frac{e^{ik_{x_s}(x''-x_s)}e^{ik_{y_s}(y''-y_s)}e^{ik_{z_s}(z''-z_s)}}{k_0^2-k_{x_s}^2-k_{y_s}^2-k_{z_s}^2}. \end{aligned} \tag{70}$$

Collecting the exponentials in x' and y' and performing the integrations with respect to these variables produces delta functions $2\pi\delta(k_{x_s}-k_{x_g})$ and $2\pi\delta(k_{y_s}-k_{y_g})$ (LHS) and $2\pi\delta(k_{x''}-k_{x_g})$ and $2\pi\delta(k_{y''}-k_{y_g})$ (RHS) allowing for the k_{x_s} and k_{y_s} (LHS) and $k_{x''}$ and $k_{y''}$ (RHS) integrals, respectively, to be carried out:

$$\begin{aligned} LHS \to & \frac{1}{(2\pi)^4}\underbrace{\int_{-\infty}^{\infty} dx'}\underbrace{\int_{-\infty}^{\infty} dy'} \int_{-\infty}^{\infty} dz' \int_{-\infty}^{\infty} dk_{z'} \frac{e^{ik_{z'}(z_g-z')}}{k_0^2-k_{x_g}^2-k_{y_g}^2-k_{z'}^2} \\ & \times k_0^2\alpha_2(z') \int_{-\infty}^{\infty} dk_{x_s} \int_{-\infty}^{\infty} dk_{y_s} \int_{-\infty}^{\infty} dk_{z_s} \underbrace{e^{i(k_{x_s}-k_{x_g})x'}}\underbrace{e^{i(k_{y_s}-k_{y_g})y'}} \\ & \times \frac{e^{-ik_{x_s}x_s}e^{-ik_{y_s}y_s}e^{ik_{z_s}(z'-z_s)}}{k_0^2-k_{x_s}^2-k_{y_s}^2-k_{z_s}^2} \\ \to & \frac{1}{(2\pi)^2}\int_{-\infty}^{\infty} dz' \int_{-\infty}^{\infty} dk_{z'} \frac{e^{ik_{z'}(z_g-z')}}{k_0^2-k_{x_g}^2-k_{y_g}^2-k_{z'}^2} k_0^2\alpha_2(z') \\ & \times \int_{-\infty}^{\infty} dk_{z_s} \frac{e^{-ik_{x_g}x_s}e^{-ik_{y_g}y_s}e^{ik_{z_s}(z'-z_s)}}{k_0^2-k_{x_g}^2-k_{y_g}^2-k_{z_s}^2} \end{aligned} \tag{71}$$

$$
\begin{aligned}
RHS \rightarrow & \frac{-1}{(2\pi)^7} \underbrace{\int_{-\infty}^{\infty} dx'} \underbrace{\int_{-\infty}^{\infty} dy'} \int_{-\infty}^{\infty} dz' \int_{-\infty}^{\infty} dk_{z'} \frac{e^{ik_{z'}(z_g - z')}}{k_0^2 - k_{x_g}^2 - k_{y_g}^2 - k_{z'}^2} \\
& \times k_0^2 \alpha_1(z') \int_{-\infty}^{\infty} dx'' \int_{-\infty}^{\infty} dy'' \int_{-\infty}^{\infty} dz'' \int_{-\infty}^{\infty} dk_{x''} \int_{-\infty}^{\infty} dk_{y''} \int_{-\infty}^{\infty} dk_{z''} \\
& \times \underbrace{e^{i(k_{x''} - k_{x_g})x'}} \underbrace{e^{i(k_{y''} - k_{y_g})y'}} \frac{e^{-ik_{x''}x''} e^{-ik_{y''}y''} e^{ik_{z''}(z' - z'')}}{k_0^2 - k_{x''}^2 - k_{y''}^2 - k_{z''}^2} k_0^2 \alpha_1(z'') \\
& \times \int_{-\infty}^{\infty} dk_{x_s} \int_{-\infty}^{\infty} dk_{y_s} \int_{-\infty}^{\infty} dk_{z_s} \frac{e^{ik_{x_s}(x'' - x_s)} e^{ik_{y_s}(y'' - y_s)} e^{ik_{z_s}(z'' - z_s)}}{k_0^2 - k_{x_s}^2 - k_{y_s}^2 - k_{z_s}^2}
\end{aligned} \tag{72}
$$

$$
\begin{aligned}
\rightarrow & \frac{-1}{(2\pi)^5} \int_{-\infty}^{\infty} dz' \int_{-\infty}^{\infty} dk_{z'} \frac{e^{ik_{z'}(z_g - z')}}{k_0^2 - k_{x_g}^2 - k_{y_g}^2 - k_{z'}^2} k_0^2 \alpha_1(z') \\
& \times \int_{-\infty}^{\infty} dx'' \int_{-\infty}^{\infty} dy'' \int_{-\infty}^{\infty} dz'' \int_{-\infty}^{\infty} dk_{z''} \\
& \times \frac{e^{-ik_{x_g}x''} e^{-ik_{y_g}y''} e^{ik_{z''}(z' - z'')}}{k_0^2 - k_{x_g}^2 - k_{y_g}^2 - k_{z''}^2} k_0^2 \alpha_1(z'') \\
& \times \int_{-\infty}^{\infty} dk_{x_s} \int_{-\infty}^{\infty} dk_{y_s} \int_{-\infty}^{\infty} dk_{z_s} \frac{e^{ik_{x_s}(x'' - x_s)} e^{ik_{y_s}(y'' - y_s)} e^{ik_{z_s}(z'' - z_s)}}{k_0^2 - k_{x_s}^2 - k_{y_s}^2 - k_{z_s}^2}
\end{aligned} \tag{73}
$$

As in the inversion for α_1, the two wavenumber integrals (over $k_{z'}$ and k_{z_s}) on the left-hand side can now be evaluated:

$$
\begin{aligned}
LHS \rightarrow & \frac{k_0^2}{(2\pi)^2} e^{-ik_{x_g}x_s} e^{-ik_{y_g}y_s} \int_{-\infty}^{\infty} dz' \alpha_2(z') \left(- \int_{-\infty}^{\infty} dk_{z'} \frac{e^{ik_{z'}(z_g - z')}}{(k_{z'} - q_g)(k_{z'} + q_g)} \right) \\
& \times \left(- \int_{-\infty}^{\infty} dk_{z_s} \frac{e^{ik_{z_s}(z' - z_s)}}{(k_{z_s} - q_g)(k_{z_s} + q_g)} \right) \\
\rightarrow & \frac{k_0^2}{(2\pi)^2} e^{-ik_{x_g}x_s} e^{-ik_{y_g}y_s} \int_{-\infty}^{\infty} dz' \alpha_2(z') \left(\frac{\pi i}{q_g} e^{iq_g|z_g - z'|} \right) \left(\frac{\pi i}{q_g} e^{iq_g|z' - z_s|} \right) \\
\rightarrow & \frac{-k_0^2}{4q_g^2} e^{-ik_{x_g}x_s} e^{-ik_{y_g}y_s} e^{-iq_g(z_g + z_s)} \int_{-\infty}^{\infty} dz' \alpha_2(z') e^{2iq_g z'}.
\end{aligned} \tag{74}
$$

Meanwhile, the right-hand side can be simplified:

$$
\begin{aligned}
RHS \rightarrow & \frac{-1}{(2\pi)^5} \int_{-\infty}^{\infty} dz' \underbrace{\int_{-\infty}^{\infty} dk_{z'} \frac{e^{ik_{z'}(z_g - z')}}{k_0^2 - k_{x_g}^2 - k_{y_g}^2 - k_{z'}^2}} k_0^2 \alpha_1(z') \int_{-\infty}^{\infty} dx'' e^{-ik_{x_g}x''} \\
& \times \int_{-\infty}^{\infty} dy'' e^{-ik_{y_g}y''} \int_{-\infty}^{\infty} dz'' \underbrace{\int_{-\infty}^{\infty} dk_{z''} \frac{e^{ik_{z''}(z' - z'')}}{k_0^2 - k_{x_g}^2 - k_{y_g}^2 - k_{z''}^2}} k_0^2 \alpha_1(z'') \\
& \times \int_{-\infty}^{\infty} dk_{x_s} e^{ik_{x_s}(x'' - x_s)} \int_{-\infty}^{\infty} dk_{y_s} e^{ik_{y_s}(y'' - y_s)} \underbrace{\int_{-\infty}^{\infty} dk_{z_s} \frac{e^{ik_{z_s}(z'' - z_s)}}{k_0^2 - k_{x_s}^2 - k_{y_s}^2 - k_{z_s}^2}}
\end{aligned} \tag{75}
$$

where

$$\int_{-\infty}^{\infty} dk_{z'} \frac{e^{ik_{z'}(z_g-z')}}{k_0^2-k_{x_g}^2-k_{y_g}^2-k_{z'}^2} = -\frac{\pi i}{q_g} e^{iq_g|z_g-z'|} \tag{76}$$

$$\int_{-\infty}^{\infty} dk_{z''} \frac{e^{ik_{z''}(z'-z'')}}{k_0^2-k_{x_g}^2-k_{y_g}^2-k_{z''}^2} = -\frac{\pi i}{q_g} e^{iq_g|z'-z''|} \tag{77}$$

$$\int_{-\infty}^{\infty} dk_{z_s} \frac{e^{ik_{z_s}(z''-z_s)}}{k_0^2-k_{x_s}^2-k_{y_s}^2-k_{z_s}^2} = -\frac{\pi i}{q_s} e^{iq_s|z''-z_s|}. \tag{78}$$

Substituting (76)–(78) into (75) yields

$$\begin{aligned} RHS \rightarrow & \frac{-1}{(2\pi)^5} \int_{-\infty}^{\infty} dz' \left(-\frac{\pi i}{q_g} e^{iq_g(z'-z_g)}\right) k_0^2 \alpha_1(z') \int_{-\infty}^{\infty} dx'' e^{-ik_{x_g}x''} \\ & \times \int_{-\infty}^{\infty} dy'' e^{-ik_{y_g}y''} \int_{-\infty}^{\infty} dz'' \left(-\frac{\pi i}{q_g} e^{iq_g|z'-z''|}\right) k_0^2 \alpha_1(z'') \\ & \times \int_{-\infty}^{\infty} dk_{x_s} e^{ik_{x_s}(x''-x_s)} \int_{-\infty}^{\infty} dk_{y_s} e^{ik_{y_s}(y''-y_s)} \left(-\frac{\pi i}{q_s} e^{iq_s(z''-z_s)}\right) \end{aligned} \tag{79}$$

and the integrations over x'' and y'' produce two more delta functions $2\pi\delta(k_{x_s}-k_{x_g})$ and $2\pi\delta(k_{y_s}-k_{y_g})$

$$\begin{aligned} RHS \rightarrow & \frac{-1}{(2\pi)^3} \int_{-\infty}^{\infty} dz' \left(-\frac{\pi i}{q_g} e^{iq_g(z'-z_g)}\right) k_0^2 \alpha_1(z') \int_{-\infty}^{\infty} dz'' \left(-\frac{\pi i}{q_g} e^{iq_g|z'-z''|}\right) k_0^2 \alpha_1(z'') \\ & \times e^{-ik_{x_g}x_s} e^{-ik_{y_g}y_s} \left(-\frac{\pi i}{q_s} e^{iq_g(z''-z_s)}\right). \end{aligned} \tag{80}$$

Then expanding the absolute value in the exponential and simplifying:

$$\begin{aligned} RHS \rightarrow & \frac{-ik_0^4}{8q_g^3} \int_{-\infty}^{\infty} dz' e^{iq_g(z'-z_g)} \alpha_1(z') \left(\int_{-\infty}^{\infty} dz'' H(z'-z'') e^{iq_g(z'-z'')} \alpha_1(z'')\right. \\ & \left. + \int_{-\infty}^{\infty} dz'' H(z''-z') e^{iq_g(z''-z')} \alpha_1(z'')\right) e^{-ik_{x_g}x_s} e^{-ik_{y_g}y_s} e^{iq_g(z''-z_s)} \\ \rightarrow & \frac{-ik_0^4}{8q_g^3} e^{-ik_{x_g}x_s} e^{-ik_{y_g}y_s} e^{-iq_g(z_g+z_s)} \int_{-\infty}^{\infty} dz' \alpha_1(z') \\ & \times \left(2\int_{-\infty}^{\infty} dz'' H(z'-z'') e^{iq_g(z'-z'')} \alpha_1(z'')\right) e^{iq_g(z'+z'')} \\ \rightarrow & \frac{-ik_0^4}{4q_g^3} e^{-ik_{x_g}x_s} e^{-ik_{y_g}y_s} e^{-iq_g(z_g+z_s)} \int_{-\infty}^{\infty} dz' \alpha_1(z') e^{2iq_g z'} \\ & \times \int_{-\infty}^{\infty} dz'' H(z'-z'') \alpha_1(z''). \end{aligned} \tag{81}$$

Now equating the left-hand and right-hand sides, (74) and (81), the phases $\exp(-ik_{x_g}x_s)$, $\exp(-ik_{y_g}y_s)$ and $\exp\left(-iq_g\left(z_g+z_s\right)\right)$ cancel leaving

$$\int_{-\infty}^{\infty} dz'\alpha_2(z')e^{2iq_gz'} = \frac{ik_0^2}{q_g}\int_{-\infty}^{\infty} dz'\alpha_1(z')e^{2iq_gz'}\int_{-\infty}^{\infty} dz''H(z'-z'')\alpha_1(z''). \tag{82}$$

Integrating the right-hand side by parts

$$\begin{aligned} u =& \int_{-\infty}^{\infty} dz''\alpha_1(z'')H(z'-z'')\alpha_1(z') \\ dv =& \frac{ik_0^2}{q_g}e^{2iq_gz'}dz' \\ \frac{du}{dz'} =& \alpha_1^2(z') + \int_{-\infty}^{\infty} dz''\alpha_1(z'')H(z'-z'')\frac{d\alpha_1(z')}{dz'} \\ =& \alpha_1^2(z') + \int_{-\infty}^{z'} dz''\alpha_1(z'')\frac{d\alpha_1(z')}{dz'} \\ v =& \frac{k_0^2}{2q_g^2}e^{2iq_gz'} \end{aligned}$$

Therefore,

$$\begin{aligned} \int_{-\infty}^{\infty} dz'e^{2iq_gz'}\alpha_2(z') = \left[\frac{k_0^2}{2q_g^2}e^{2iq_gz'}\int_{-\infty}^{\infty} dz''\alpha_1(z'')H(z'-z'')\alpha_1(z')\right]_{z'=-\infty}^{\infty} \\ - \int_{-\infty}^{\infty} dz'e^{2iq_gz'}\frac{k_0^2}{2q_g^2}\left(\alpha_1^2(z') + \int_{-\infty}^{z'} dz''\alpha_1(z'')\frac{d\alpha_1(z')}{dz'}\right), \end{aligned} \tag{83}$$

the boundary terms are zero (assuming α_1, like α, is confined to a finite region) and so

$$\tilde{\alpha}_2(-2q_g) = -\int_{-\infty}^{\infty} dz'e^{2iq_gz'}\frac{k_0^2}{2q_g^2}\left(\alpha_1^2(z') + \int_{-\infty}^{z'} dz''\alpha_1(z'')\frac{d\alpha_1(z')}{dz'}\right). \tag{84}$$

Performing an inverse Fourier transform and holding the angle of incidence constant gives

$$\alpha_2(z,\theta_0) = -\frac{1}{2\cos^2\theta_0}\left(\alpha_1^2(z,\theta_0) + \int_{-\infty}^{z} \alpha_1(z',\theta_0)dz'\frac{\partial\alpha_1(z,\theta_0)}{\partial z}\right) \tag{85}$$

C Isolation of the leading order imaging portion from the third term, α_3

For a detailed derivation and separation of the third term in the inverse series, the reader is referred to the appendices of Shaw et al. (2003). For the purposes of this paper, we include only the steps taken to get to the generalized constant θ_0 form. The integral equation to be solved for the third term in the series is

$$\begin{aligned}
&\int_{-\infty}^{\infty} d\vec{x}'\, G_0\left(\vec{x}_g|\vec{x}';\omega\right) k_0^2\alpha_3(z')G_0\left(\vec{x}'|\vec{x}_s;\omega\right)\\
&\qquad = -\int_{-\infty}^{\infty} d\vec{x}'\, G_0\left(\vec{x}_g|\vec{x}';\omega\right) k_0^2\alpha_1(z')\\
&\qquad\quad \times \int_{-\infty}^{\infty} d\vec{x}''\, G_0\left(\vec{x}'|\vec{x}'';\omega\right) k_0^2\alpha_2(z'')G_0\left(\vec{x}''|\vec{x}_s;\omega\right)\\
&\qquad\quad -\int_{-\infty}^{\infty} d\vec{x}'\, G_0\left(\vec{x}_g|\vec{x}';\omega\right) k_0^2\alpha_2(z')\\
&\qquad\quad \times \int_{-\infty}^{\infty} d\vec{x}''\, G_0\left(\vec{x}'|\vec{x}'';\omega\right) k_0^2\alpha_1(z'')G_0\left(\vec{x}''|\vec{x}_s;\omega\right)\\
&\qquad\quad -\int_{-\infty}^{\infty} d\vec{x}'\, G_0\left(\vec{x}_g|\vec{x}';\omega\right) k_0^2\alpha_1(z')\\
&\qquad\quad \times \int_{-\infty}^{\infty} d\vec{x}''\, G_0\left(\vec{x}'|\vec{x}'';\omega\right) k_0^2\alpha_1(z'')\\
&\qquad\quad \times \int_{-\infty}^{\infty} d\vec{x}'''\, G_0\left(\vec{x}''|\vec{x}''';\omega\right) k_0^2\alpha_1(z''')G_0\left(\vec{x}'''|\vec{x}_s;\omega\right). \qquad (86)
\end{aligned}$$

Fourier transform both sides of (86) over x_g and y_g and following the same steps as in deriving (74), the left-hand side of (86) becomes

$$LHS \rightarrow \frac{-k_0^2}{4q_g^2} e^{-ik_{x_g}x_s} e^{-ik_{y_g}y_s} e^{-iq_g(z_g+z_s)} \int_{-\infty}^{\infty} \alpha_3(z') e^{2iq_g z'} dz'. \qquad (87)$$

Meanwhile, the right-hand side becomes

$$\begin{aligned}
RHS \rightarrow & -\frac{ik_0^4}{4q_g^3} e^{-ik_{x_g}x_s} e^{-ik_{y_g}y_s} e^{-iq_g(z_g+z_s)} \int_{-\infty}^{\infty} dz' \underline{\alpha_1}(z') \int_{-\infty}^{\infty} dz'' H(z'-z'') \underline{\alpha_2}(z'') e^{2iq_g z'}\\
& -\frac{ik_0^4}{4q_g^3} e^{-ik_{x_g}x_s} e^{-ik_{y_g}y_s} e^{-iq_g(z_g+z_s)} \int_{-\infty}^{\infty} dz' \underline{\alpha_2}(z') \int_{-\infty}^{\infty} dz'' H(z'-z'') \underline{\alpha_1}(z'') e^{2iq_g z'}\\
& -\frac{k_0^4}{(2\pi)^4} e^{-ik_{x_g}x_s} e^{-ik_{y_g}y_s} \int_{-\infty}^{\infty} dz' \int_{-\infty}^{\infty} dk_{z'} \frac{e^{ik_{z'}(z_g-z')}}{k_0^2 - k_{x_g}^2 - k_{y_g}^2 - k_{z'}^2}\\
& \times \alpha_1(z') \int_{-\infty}^{\infty} dz'' \int_{-\infty}^{\infty} dk_{z''} \frac{e^{ik_{z''}(z'-z'')}}{k_0^2 - k_{x_g}^2 - k_{y_g}^2 - k_{z''}^2} \alpha_1(z'')\\
& \times \int_{-\infty}^{\infty} dz''' \int_{-\infty}^{\infty} dk_{z'''} \frac{e^{ik_{z'''}(z''-z''')}}{k_0^2 - k_{x_g}^2 - k_{y_g}^2 - k_{z_g}^2} \alpha_1(z''') \int_{-\infty}^{\infty} dk_{z_s} \frac{e^{ik_{z_s}(z'''-z_s)}}{k_0^2 - k_{x_g}^2 - k_{y_g}^2 - k_{z_s}^2}.
\end{aligned}$$

(88)

Simplifying gives

$$
\begin{aligned}
\int_{-\infty}^{\infty} \alpha_3(z')e^{2iq_g z'}dz' =& \frac{ik_0^2}{q_g}\int_{-\infty}^{\infty} dz'\alpha_1(z')\int_{-\infty}^{\infty} dz'' H(z'-z'')\alpha_2(z'')e^{2iq_g z'} \\
& \frac{ik_0^2}{q_g}\int_{-\infty}^{\infty} dz'\alpha_2(z')\int_{-\infty}^{\infty} dz'' H(z'-z'')\alpha_1(z'')e^{2iq_g z'} \\
& + \frac{k_0^2}{4q_g^2}\int_{-\infty}^{\infty} dz' e^{iq_g z'}\alpha_1(z')\int_{-\infty}^{\infty} dz'' e^{iq_g|z'-z''|}\alpha_1(z'') \\
& \int_{-\infty}^{\infty} dz''' e^{iq_g|z''-z'''|}\alpha_1(z''')e^{iq_g z'''}. \qquad (89)
\end{aligned}
$$

Then, integrating by parts and inverse Fourier transforming holding θ_0 constant gives

$$
\begin{aligned}
\alpha_3(z,\theta_0) =& \frac{-k_0^2}{q_g^2}\alpha_1(z,\theta_0)\alpha_2(z,\theta_0) - \frac{-k_0^2}{2q_g^2}\alpha_1(z,\theta_0)\int_{-\infty}^{z}\alpha_2(z',\theta_0)dz'\frac{\partial\alpha_1(z,\theta_0)}{\partial z} \\
& - \frac{k_0^2}{2q_g^2}\alpha_2(z,\theta_0)\int_{-\infty}^{z}\alpha_1(z',\theta_0)dz'\frac{\partial\alpha_2(z,\theta_0)}{\partial z} \\
& - \frac{k_0^2}{4q_g^2}\int_{-\infty}^{\infty} dz'\int_{-\infty}^{\infty} dz''\int_{-\infty}^{\infty} dz'''\alpha_1(z',\theta_0)\alpha_1(z'',\theta_0)\alpha_1(z'',\theta_0) \\
& \times \Big(H(z'-z'')H(z''-z''')e^{2iq_g z'}e^{-iq_g z'''} \\
& + H(z'-z'')H(z'''-z'')e^{iq_g z'}e^{-2iq_g z''}e^{iq_g z'''} \\
& + H(z''-z')H(z''-z''')e^{-iq_g z'}e^{2iq_g z''}e^{-iq_g z'''} \\
& + H(z''-z')H(z'''-z'')e^{-iq_g z'}e^{iq_g z'''}\Big). \qquad (90)
\end{aligned}
$$

By comparison with the 1-D normal incidence derivation (Shaw et al., 2003; Innanen, 2003),

$$
\begin{aligned}
\alpha_3(z,\theta_0) =& \frac{1}{\cos^4\theta_0}\left(\frac{3}{16}\alpha_1^3(z,\theta_0) + \frac{1}{8}\left(\int_{-\infty}^{z}\alpha_1(z',\theta_0)dz'\right)^2\left[\frac{\partial^2}{\partial z^2}\alpha_1(z,\theta_0)\right]\right. \\
& + \frac{5}{8}\alpha_1(z,\theta_0)\int_{-\infty}^{z}\alpha_1(z',\theta_0)dz'\left[\frac{\partial}{\partial z}\alpha_1(z,\theta_0)\right] \\
& + \frac{1}{8}\left[\frac{\partial}{\partial z}\alpha_1(z,\theta_0)\right]\int_{-\infty}^{z}\left(\int_{-\infty}^{z'}\alpha_1(z'',\theta_0)dz''\left[\frac{\partial}{\partial z'}\alpha_1(z',\theta_0)\right]\right)dz' \\
& \left. -\frac{1}{16}\int_{-\infty}^{z}\int_{-\infty}^{z}\left[\frac{\partial}{\partial z'}\alpha_1(z',\theta_0)\right]\left[\frac{\partial}{\partial z''}\alpha_1(z'',\theta_0)\right]\alpha_1(z''+z'-z,\theta_0)dz''dz'\right) \qquad (91)
\end{aligned}
$$

and the amplitude-only and leading order imaging contributions are

$$
\alpha_3(z,\theta_0) = \frac{3}{16}\frac{1}{\cos^4\theta_0}\alpha_1^3(z,\theta_0) + \frac{1}{8}\frac{1}{\cos^4\theta_0}\left(\int_{-\infty}^{z}\alpha_1(z',\theta_0)dz'\right)^2\frac{\partial^2\alpha_1(z,\theta_0)}{\partial z^2} + \cdots \qquad (92)
$$

respectively.